https://doi.org/10.5194/egusphere-2025-441
Preprint. Discussion started: 12 March 2025
© Author(s) 2025. CC BY 4.0 License.

Competing processes determine the long-term impact of basal friction parameterizations for Antarctic mass loss

Tim van den Akker[1], William H. Lipscomb[2], Gunter R. Leguy[2], Willem Jan van de Berg[1], Roderik S.W. van de Wal[1,3]

[1]Institute for Marine and Atmospheric Research Utrecht, Utrecht University, Netherlands
[2]Climate and Global Dynamics Laboratory, NSF National Center for Atmospheric Research, Boulder, CO, USA
[3]Department of Physical Geography, Utrecht University, Netherlands

Correspondence to: Tim van den Akker (t.vandenakker@uu.nl)

Abstract. An often-mentioned source of uncertainty when projecting future sea level rise with ice sheet models is the choice of basal friction law. Previous studies do not agree on whether this choice causes significantly different projections. We use the Community Ice Sheet Model (CISM) to show that the sensitivity of the projected sea level rise to the choice of basal friction law depends on the geometric setting and the inversion procedure: CISM can be tuned to be sensitive to the choice of basal friction law or not. We find a geometry-driven connection between buttressing and basal sliding in the Amundsen Sea Embayment. When Thwaites Glacier collapses, it creates a grounding line flux large enough to sustain an ice shelf that provides buttressing and reduces the importance of basal friction. This is not the case, however, when Pine Island Glacier retreats significantly. Thus, a collapsing Pine Island glacier is sensitive to the choice of basal friction law, but a collapsing Thwaites Glacier is not. Which glacier collapses first depends on the inversion procedure. This study highlights the importance of the initialization procedure, and the underdetermined nature of ice sheet modelling. The latter makes it difficult to base general claims on ice sheet modelling results.

1 Introduction

The projected Antarctic contribution to global mean sea level (GMSL) rise ranges from 0.03 - 0.27 m (SSP1.9) to 0.03 - 0.34 m (SSP8.5) in 2100 (Fox-Kemper et al., 2021). After 2100, uncertainty increases because of dynamical processes, leading to a possible multi-meter GMSL rise by 2300 (Fox-Kemper et al., 2021; Payne et al., 2021; Seroussi et al., 2024). By and after 2300, self-sustaining processes could cause the deglaciation of large parts of the West Antarctic Ice Sheet (WAIS) (Joughin et al., 2014; Cornford et al., 2015; Seroussi et al., 2017; Coulon et al., 2024; Van Den Akker et al., 2024).

The largest dynamic mass changes are currently ongoing in the Amundsen Sea Embayment (ASE) (Smith et al., 2020). The possible deglaciation of the two largest glaciers in this region, Pine Island Glacier (PIG) and the Thwaites Glacier (TG), is therefore a main source of uncertainty in future simulations (Arthern and Williams, 2017; Bett et al., 2023; Cornford et al.,

https://doi.org/10.5194/egusphere-2025-441
Preprint. Discussion started: 12 March 2025
© Author(s) 2025. CC BY 4.0 License.

2015; Feldmann and Levermann, 2015; Pattyn and Morlighem, 2020; Seroussi et al., 2024). The grounding line of both glaciers rests on a retrograde bed, making them susceptible to the Marine Ice Sheet Instability (MISI, see Schoof (2007b)). Some studies (Joughin et al., 2014; Favier et al., 2014) suggest that those glaciers are already undergoing MISI-like retreat. Recent studies suggested that present-day ocean temperatures could drive complete deglaciation of this area over several centuries, without additional warming (Reese et al., 2023; Van Den Akker et al., 2024).

Sources of modelled ice sheet uncertainty could be missing representation of certain physical processes, or a suboptimal initial state (Aschwanden et al., 2021). Several studies have attributed uncertainty in sea level prediction from ice sheet models to the choice of the basal friction parameterization (Sun et al., 2020; Brondex et al., 2017; Brondex et al., 2019; Wernecke et al., 2022; Barnes and Gudmundsson, 2022; Joughin et al., 2024; Berdahl et al., 2023; Bulthuis et al., 2019). These parameterizations are relations between ice basal velocities and the friction at the ice-bedrock interface. Generally, the existing relations, or basal friction laws, can be separated into two categories. The first category is a relation where friction depends on the basal velocity raised to some power. Using an exponent of 1 results in a linear relation, but exponents between 0 and 1 are more common (Weertman, 1957; Budd et al., 1979; Barnes and Gudmundsson, 2022; Das et al., 2023). These are referred to as ‘power law friction’. The second category is a relation in which the friction becomes independent of velocity for fast- flowing ice. This is referred to as ‘Coulomb friction’ (Joughin et al., 2019; Tsai et al., 2015; Zoet and Iverson, 2020; Schoof, 2005). Both types of basal friction laws usually contain free parameters that can be tuned to match observed quantities such as ice sheet surface velocities or thickness.

Another source of uncertainty is the potential of ice shelves to provide a buttressing force on the inland ice sheet (Dupont and Alley, 2005; Gudmundsson, 2013; Haseloff and Sergienko, 2018; Reese et al., 2018a; Fürst et al., 2016). A buttressed ice shelf can act as plug against glacier acceleration. An accelerating glacier has an increasing grounding line flux, transporting more ice to the ice shelf. If the thicker shelf can persist, this will increase its buttressing capacity and oppose the initial acceleration of the inland ice. Choices related to basal friction will influence both the velocity profile and the modelled buttressing of simulated ice sheets.

Most of the literature cited here argues that power law friction will result in less modelled sea level rise compared to Coulomb friction, both for idealized experiments (e.g. MISMIP-style experiments, see Asay-Davis et al. (2016)) and for realistic simulations of the Antarctic Ice Sheet (AIS). However, authors do not agree if the difference is substantial (e.g., Brondex et al. (2017); Sun et al. (2020); Brondex et al. (2019) or not (e.g., (Barnes and Gudmundsson, 2022; Wernecke et al., 2022). Furthermore, basal friction parameterization tests in realistic settings such as the ASE or the entire AIS are often done with enormous (ABUMIP, Sun et al. (2020) or unrealistic perturbations (Barnes and Gudmundsson, 2022; Brondex et al., 2019). Tests with realistic forcing and therefore realistic mass change rates, as well as a more generic study of the importance of these factors for long-term WAIS collapse, are missing.

https://doi.org/10.5194/egusphere-2025-441
Preprint. Discussion started: 12 March 2025
© Author(s) 2025. CC BY 4.0 License.

Here we use the Community Ice Sheet Model (CISM) (Lipscomb et al., 2019; Lipscomb et al., 2021) to investigate the sensitivity of grounding line retreat and ice mass loss to the choice of basal friction laws for the West Antarctic Ice Sheet, showing the importance of ice-shelf buttressing. Building on the work of Brondex et al. (2017) and Brondex et al. (2019), we extend our simulations for 2000 years into the future, to capture the importance of significant grounding line retreat. We use the observed mass change rates from Smith et al. (2020) as perturbation, applied in the same way as in Van Den Akker et al. (2025). We perform two initializations: one where we tune free parameters in the basal friction laws to nudge the modelled ice sheet thickness toward observations, and one where we additionally tune a flow enhancement factor to nudge the modelled ice surface velocities closer to observations. We then continue our simulations with four widely used friction laws. We show that the modelled sensitivity to the choice of basal friction parameterization is determined by the geometry of the evolving ice sheet. Some geometries allow for compensating effects between buttressing and basal friction. The geometry is in turn determined by the initialization. Hence, we show that the ice sheet model can be initialized to be sensitive to the choice of basal friction law or not.

2 Methods

2.1 Basal friction

We test four basal friction laws. First, we use a Coulomb sliding law proposed by Zoet and Iverson (2020):

$$\tau_{b,Reg} = \beta u_b = C_c N \left(\frac{u_b}{u_b + u_0}\right)^{\frac{1}{m}} \quad (1.1)$$

where $\tau_{b,Reg}$ is the basal friction, β is the basal friction divided by the ice basal velocity u_b (the implementation in CISM), is N the effective pressure, C_c is a unitless parameter in the range [0,1] controlling the strength of the Coulomb sliding, u_0 is the yield velocity and m a modeler-defined exponent (usually chosen to be 3). For their short description and units, see Table 1 and 2. The spatial-varying parameter C_c corresponds to $tan\,\phi$ of Zoet and Iverson (2020), in which ϕ is the friction angle, a material property of the subglacial till. This parameter is used to nudge our modelled ice sheet toward the observed ice thickness by a process described in the next section.

In addition to the Zoet-Iverson friction law, we consider three more relations:

$$\tau_{b,Powerlaw} = C_p * u_b^{\frac{1}{m}} \quad (1.2)$$

https://doi.org/10.5194/egusphere-2025-441
Preprint. Discussion started: 12 March 2025
© Author(s) 2025. CC BY 4.0 License.

$$\tau_{b,Schoof} = \frac{C_p C_c N}{\left[C_p^m u_b + (C_c N)^{\mathrm{m}}\right]^{\frac{1}{m}}} u_b^{\frac{1}{m}} \quad (1.3)$$

$$\tau_{b,Pseudoplastic} = C_c N \left(\frac{u_b}{u_0}\right)^{\frac{1}{pp}} \quad (1.4)$$

In these equations, C_p is a possibly spatially varying constant. Eq. 1.2 is the classical power law for sliding ('power law' hereafter) from Weertman (1957). Note that this m is the same as in Eq 1.1; it regulates the strength of the power law friction. Eq 1.3, often referred to as the "Schoof law" (Schoof, 2005), is a regularized Coulomb friction law suggested for the Marine Ice Sheet Model Intercomparison Project third phase (MISMIP+) experiments (Asay-Davis et al., 2016) and used in CISM in Lipscomb et al. (2021). It is argued in the literature that Eq 1.3 is preferred over Eq 1.2 because it yields physically realistic behavior of a retreating glacier (Brondex et al., 2017; Brondex et al., 2019). Eq 1.4 and is referred to as a 'pseudoplastic' law, developed and used by Winkelmann et al. (2011); Aschwanden et al. (2016). This last sliding law is similar in behavior to the power law but includes the effective pressure N, as in Eq. 1.3 and a value for m between 1 and 5.

The effective pressure N at the ice–bed interface is the difference between the ice overburden pressure and the subglacial water pressure. In our simulations, the effective pressure is lowered near grounding lines to represent the connection of the subglacial hydrological system to the ocean (Leguy et al., 2014):

$$N = \rho_i g H \left(1 - \frac{H_f}{H}\right)^p \quad (1.5)$$

Where ρ_i is the density of glacial ice, g the gravitational acceleration, H the ice thickness and p is a number in the range [0,1]. The flotation thickness H_f is the height of an ice column resting on bedrock below sea level (b < 0) at hydrostatic equilibrium, which is given by:

$$H_f = \max\left(0, -\frac{\rho_w}{\rho_i} b\right) \quad (1.6)$$

where ρ_w is the sea water density, and b is the bedrock height. Simulations in this study were done with $p = 0.5$ unless stated otherwise. At the grounding line, we apply friction and/or basal melt scaled by the percentage of the modelled grid cell that is grounded as in Leguy et al. (2021).

https://doi.org/10.5194/egusphere-2025-441
Preprint. Discussion started: 12 March 2025
© Author(s) 2025. CC BY 4.0 License.

The four friction laws differ in their dependence on the ice basal velocities and are shown with typical values in Fig. 1. The power law and the pseudoplastic law differ clearly from the Schoof and Zoet-Iverson law as they do not asymptote for high basal velocity. The Schoof and Zoet-Iverson law behave similarly, although the Zoet-Iverson law is slightly more sensitive to changes in velocity. The power law and pseudoplastic law show increasing basal friction with increasing velocity. This introduces a negative feedback: a decrease in friction initially increases velocity, which in the power law and pseudoplastic law will always increase the friction. In the other two laws, the basal friction asymptotes for high velocities to $C_c N$, which is pure Coulomb friction.

Three of the sliding laws depend on the effective pressure. This introduces a feedback between ice velocities and basal friction. If the basal friction decreases, the ice flux across the grounding line increases. This decreases the ice thickness upstream of the grounding line, further reducing N. Thinning grounded ice, for example caused by a loss of buttressing, can lower N and lead to thinning far upstream of the grounding line (Brondex et al., 2017; Brondex et al., 2019).

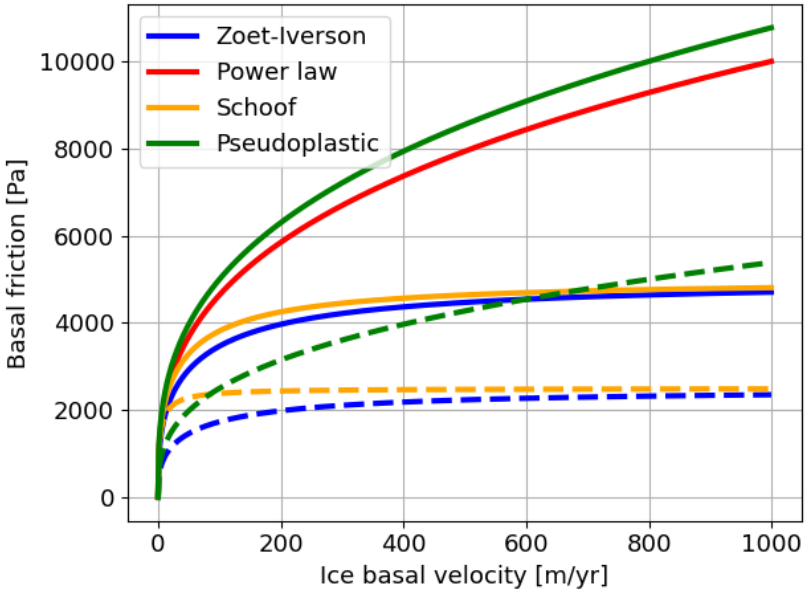

Figure 1. The friction laws with indicative values. Basal friction as function of the ice basal velocity for constant values of $C_c = 0.5$, $C_p = 1000$, $N = 10000$ Pa, $u_0 = 250$ m/yr, and $m = 3$. Dashed lines are the same basal friction laws with N=5000 Pa. The power law is independed on N, so the solid and dashed red line are the same.

2.2 Buttressing

We quantify the buttressing capacity of an ice shelf at the grounding line with two approaches. The first approach compares the linearized stress balance at the grounding line to the stress boundary condition at the calving front. This buttressing number,

https://doi.org/10.5194/egusphere-2025-441
Preprint. Discussion started: 12 March 2025
© Author(s) 2025. CC BY 4.0 License.

defined as the ratio between the latter two stresses, has been used in several studies (Gudmundsson, 2013; Gudmundsson et al., 2023; Fürst et al., 2016) and as a parameter in the analytical grounding line flux of Schoof (2007a) and Schoof (2007b). Reese et al. (2018a) describe three ways to calculate the buttressing number, of which we choose and adapt Eq. 1 following Fürst et al. (2016):

$$\chi = 1 - \frac{\boldsymbol{n_1}.\boldsymbol{R}\boldsymbol{n_1}}{2\chi_f} \tag{1.7}$$

The vector $\boldsymbol{n_1}$ is the vector perpendicular to the grounding line, in our regular rectangular grid best approximated by the direction of the ice flow. The stress boundary condition at the calving front χ_f is given by

$$\chi_f = \frac{\rho_i g}{4}(1 - \frac{\rho_i}{\rho_w})H \tag{1.8}$$

The resistive stress tensor $\boldsymbol{R}$ is given by

$$\boldsymbol{R} = \begin{pmatrix} 2\tau_{xx} + \tau_{yy} & \tau_{xy} \\ \tau_{xy} & \tau_{xx} + 2\tau_{yy} \end{pmatrix} \tag{1.9}$$

With this term χ in Eq 1.7, a value of 0 denotes no buttressing: the buttressing force equals the driving stress if the ice sheet ended at that point with an ice cliff. Values above zero indicate buttressing. Values below zero point to a tensile regime where the ice shelf is pulling grounded ice over the grounding line. As shown by Reese et al. (2018a), the buttressing number from the linearized stress balance approach depends on the choice of $\boldsymbol{n_1}$ and $\boldsymbol{R}$, and assumes that the stress tensor at the grounding line is determined by the buttressing capacity of the downstream shelf only. The former assumption implies that high basal friction just upstream of the grounding line, which will brake ice flow, is interpreted as buttressing as well

The second approach to quantify the buttressing is by performing so-called shelf-kill experiments (e.g. Antarctic BUttressing Model Intercomparison Project (ABUMIP), Sun et al. (2020); Reese et al. (2018b). In these experiments, floating ice is instantly removed, and the effect on the grounded ice in terms of acceleration is used to measure the buttressing capacity of the removed shelves. We define the acceleration number, in analogy to the definition of the buttressing number, by

$$\alpha = 1 - \frac{u_{before}}{u_{after}} \tag{1.10}$$

in which u_{before} and u_{after} refer to the local depth-averaged ice velocity before and after removing the shelf. This method of quantifying the buttressing is the purest way of assessing shelf strength but provides only a temporal snapshot and requires an additional ice sheet model timestep to be calculated.

https://doi.org/10.5194/egusphere-2025-441
Preprint. Discussion started: 12 March 2025
© Author(s) 2025. CC BY 4.0 License.

Both methods shown in Eqs 1.7 and 1.10 are tested on a theoretical case (the Ice1r experiment of MISMIP+, see Asay-Davis et al. (2016) and on the present-day state of the Antarctic Ice Sheet, before using them in the continuation simulations in this study. These results for the buttressing can be found in the supplementary material, Fig S1-S3. We find high buttressing numbers in the center of the confined fjord and low buttressing numbers (tensile regimes) at the outer fjord boundaries, as would be expected. Furthermore, the acceleration number and buttressing number correlate well, i.e. a high buttressing number corresponds to a high acceleration number.

2.3 The Community Ice Sheet Model

The Community Ice Sheet Model is a thermo-mechanical higher-order ice sheet model, which is part of the Community Earth System Model version 2 (CESM2, Danabasoglu et al. (2020). Earlier applications of CISM to the Antarctic Ice Sheet retreat can be found in Seroussi et al. (2020); Lipscomb et al. (2021); Berdahl et al. (2023); Van Den Akker et al. (2025). The variables and constants used in the text and equations below are listed in Tables 1 and 2.

Table 1. Variables used in this study.

Variables	Definition
b	Bedrock height [m asl]
$bmlt$	Basal melt rate under floating ice [m/yr]
C_c	Coulomb C [unitless]
C_p	Power law C [Pa $m^{1/m}$ $yr^{-1/m}$]
C_r	Basal friction relaxation target [unitless]
E	Flow enhancement factor [unitless]
E_r	Flow enhancement factor relaxation target [unitless]
H	Modelled ice thickness [m]
H_f	Ice thickness above floatation [m]
H_{obs}	Observed ice thickness [m]
N	Effective pressure [Pa]
R	Resistive stress tensor [Pa]
R_n	Normal resistive stress tensor at grounding line [Pa]
R_0	Resistive stress tensor without ice [Pa]
TF_{base}	Thermal forcing applied at the ice shelf draft [K]
u	Ice velocity in the x-direction [m/yr]

https://doi.org/10.5194/egusphere-2025-441
Preprint. Discussion started: 12 March 2025
© Author(s) 2025. CC BY 4.0 License.

v	Ice velocity in the y-direction [m/yr]
u_b	Basal velocity magnitude [m/yr]
$u_{x,b}$	Basal velocity in the x-direction [m/yr]
$u_{y,b}$	Basal velocity in the y-direction [m/yr]
u_s	Surface ice velocity magnitude [m/yr]
$u_{s,obs}$	Observed surface ice velocity magnitude [m/yr]
δT	Ocean temperature correction [K]
s	Surface elevation [m]
β	Basal traction parameter [Pa yr m^{-1}]
ϕ	Till friction angle [degrees]
η	Effective viscosity [Pa yr]
θ	Buttressing fraction [unitless]
τ_b	Basal shear stress [Pa]
τ_{ij}	Deviatoric stress tensor [Pa]
χ	Buttressing number [unitless]
χ_f	Stress boundary condition at the calving front [Pa]

Table 2. Parameters and their units and values used in this study

Parameters	Values	Units	Definition
c_{pw}	3974	J kg^{-1} K^{-1}	Specific heat of seawater
g	9.81	m s^{-2}	Gravitational acceleration
H_0	100	m	Ice thickness scale in the inversion
L_f	3.34 x 105	J kg^{-1}	Latent heat of fusion
m	3	-	Basal friction exponent
pp	5	-	Basal friction exponent, pseudoplastic law
T_r	0	K	Relaxation target of the ocean temperature inversion
u_0	200	m yr^{-1}	Constant ice speed in the Zoet-Iverson and pseudoplastic laws
p	0.5	-	Exponent in effective pressure relation

https://doi.org/10.5194/egusphere-2025-441
Preprint. Discussion started: 12 March 2025
© Author(s) 2025. CC BY 4.0 License.

r	0.5	-	Strength of inversion relaxation
ρ_i	917	kg m^{-3}	Density of ice
ρ_w	1027	kg m^{-3}	Density of ocean water
κ	100	yr	Time scale in the inversion
γ_0	30000	m yr^{-1}	Basal melt rate coefficient
A_0	1.733 x 10^3 3.613 x 10^{-13}	Pa^{-3} s^{-1}	Constant of proportionality for the rate factor (above 263 K),(below 263 K)
Q	139 x 10^3, 60 x 10^3	J mol^{-1}	Activation energy for ice creep (above 263 K), (below 263 K)
R	8.314	J mol^{-1} K^{-1}	Universal gas constant
Φ	9.8 x 10^{-8}	K Pa^{-1}	Pressure-dependent melt constant

We run CISM with a vertically integrated higher-order approximation to the momentum balance, the Depth Integrated Viscosity Approximation (DIVA) (Goldberg, 2011; Lipscomb et al., 2019; Robinson et al., 2022). The momentum balance in the x-direction is defined as:

$$\frac{\partial}{\partial x}\left(2\bar{\eta}H\left(2\frac{\partial \bar{u}}{\partial x}+\frac{\partial \bar{v}}{\partial y}\right)\right)+\frac{\partial}{\partial y}\left(\bar{\eta}H\left(\frac{\partial \bar{u}}{\partial y}+\frac{\partial \bar{v}}{\partial x}\right)\right)-\beta u_{x,b}=\rho_i g H\frac{\partial s}{\partial x} \quad (1.11)$$

The momentum balance in the y-direction is similar. Barred variables are depth averaged. Basal friction, which is parameterized in the ways described in Sec. 2.1, appears as the product of β and the directional velocity in Eqs 1.11.

Since C_c (or C_p) is poorly constrained by theory and observations, we use it as a spatially variable tuning parameter. We tune C_c using a nudging method (Lipscomb et al., 2021; Pollard and Deconto, 2012):

$$\frac{dC_c}{dt}=-C_c\left[\left(\frac{H-H_{obs}}{H_0\tau}\right)+\frac{2}{H_0}\frac{dH}{dt}-\frac{\mathrm{r}}{\kappa}ln\frac{C_c}{C_r}\right] \quad (1.12)$$

Where κ is the relaxation timescale The relaxation target C_r is a 2D field that penalizes very high and low values of C_c. It is based on elevation, with lower values at low elevation where soft marine sediments are likely more prevalent, loosely following

https://doi.org/10.5194/egusphere-2025-441
Preprint. Discussion started: 12 March 2025
© Author(s) 2025. CC BY 4.0 License.

Winkelmann et al. (2011). We chose targets of 0.1 for bedrock below -700 m asl and 0.4 for 700 m asl, with linearly interpolation in between, based on Aschwanden et al. (2013).

Basal melt rates are calculated using a local quadratic relation with a thermal forcing observational dataset (Jourdain et al., 2020):

$$bmlt = \gamma_0 \left(\frac{\rho_w c_{pw}}{\rho_i L_f}\right)^2 (\max[TF_{\text{base}} + \delta T, 0])^2 \tag{1.13}$$

where TF is the ocean thermal forcing (the difference between the ocean temperature the local melting point) from Jourdain et al. (2020). The basal melt rates are tuned in order for the floating ice to match the thickness observations of Morlighem et al. (2020), similar to Eq. 1.12 but with δT as tuning variable:

$$\frac{d(\delta T)}{dt} = -\delta T \left[\left(\frac{H - H_{obs}}{H_0 \tau}\right) + \frac{2}{H_0}\frac{dH}{dt}\right] + \frac{(\mathrm{T_r} - \delta \mathrm{T})}{\kappa} \tag{1.14}$$

As in Eq 1.12, we add a term including a relaxation target T_r to penalize large deviations. In this case, the relaxation target is zero, since δT is a temperature correction to the dataset of Jourdain et al. (2020). The melt sensitivity γ_0 is chosen to be 3.0×10^4 m/yr, which was used in Lipscomb et al. (2021) and Van Den Akker et al. (2024) to obtain basal melt rates in good agreement with observations and with a shelf-average δT close to zero in the Amundsen Sea Embayment.

Additionally, a flow enhancement factor E can be tuned to nudge modelled ice surface velocities towards observations in a similar way:

$$\frac{dE}{dt} = E\left[-\left(\frac{u_s - u_{s,obs}}{v_0 \kappa}\right) + \frac{2}{H_0}\frac{dH}{dt} + \mathrm{r}\, log\frac{E}{E_r}\right] \tag{1.15}$$

The flow enhancement factor is then used in the calculation of the rate factor A:

$$\mathrm{A} = \mathrm{E}\mathrm{A}_0 e^{-Q/(RT^*)}, \tag{1.16}$$

with T^* as the homologous temperature and A_0, Q, R as constants (see Table 2):

https://doi.org/10.5194/egusphere-2025-441
Preprint. Discussion started: 12 March 2025
© Author(s) 2025. CC BY 4.0 License.

$$T^* = T + \rho g H \Phi. \tag{1.17}$$

Then, A is used together with the strain rates ϵ to calculate the effective viscosity of the ice, η, which controls the ice velocity:

$$\eta = \frac{1}{2} A^{-\frac{1}{n}} \epsilon_e^{\frac{1-n}{n}}. \tag{1.18}$$

The effective strain rate ϵ_e is defined as the norm of the strain-rate tensor:

$$\epsilon_e = \frac{1}{2} \epsilon_{i,j} \epsilon_{i,j}, \tag{1.19}$$

with

$$\epsilon_{i,j} = \frac{1}{2} \left(\frac{\delta u_i}{\delta x_j} + \frac{\delta u_j}{\delta x_i} \right). \tag{1.20}$$

We tune for both the basal friction coefficient and the flow enhancement factor in this study. We define 'inversion' here as the process of retrieving, tuning or nudging a parameter (i.e. the flow enhancement factor) from observables (ice surface velocities). This flow enhancement factor inversion can interfere with the basal friction inversion in Eq. 1.12. For example, if the modelled ice is thinner than observed in a grid cell, the basal friction inversion tends to increase C_c via Eq. 1.12 to slow down and pile up the ice at that location. By doing this, the surface velocity decreases. If the modelled surface velocities fall below the observed velocities, the flow enhancement factor will increase to speed up the ice, counteracting the ice thickness increase caused by the basal friction inversion. This creates a conflict between the two inversions.

The basal friction inversion is the primary and default inversion. It has been successfully applied to the AIS in an ISMIP6-style (Ice Sheet Model Intercomparrison Project for CMIP6, Nowicki et al. (2016)) setting in Lipscomb et al. (2021) and Van Den Akker et al. (2024), while the flow enhancement factor inversion has been developed for this study, and is therefore less tested and validated. For this reason, whenever there is a conflict between the flow enhancement factor inversion and the basal friction inversion, we default to the basal friction inversion and turn off the flow enhancement factor inversion at that timestep and location. To prevent overfitting, the flow enhancement factor is only allowed to be changed in grid cells where the ice surface velocity mismatch is larger than 25 m yr^{-1}.

The grounding line (GL) is not explicitly modeled in CISM, but its location can be diagnosed from the hydrostatic balance. Since we use a regular rectangular grid, the modeled GL cuts through cells. To prevent abrupt jumps in the basal friction and the basal melt rates close to the GL, we use a GL parameterization (Leguy et al., 2021), where we use a flotation function to weigh the basal friction and basal melt rates according to the percentage of a grid cell that is grounded.

https://doi.org/10.5194/egusphere-2025-441
Preprint. Discussion started: 12 March 2025
© Author(s) 2025. CC BY 4.0 License.

2.4 Initializations

In this study, we use two initializations. The 'default initialization' (abbreviated as 'DI') uses the observed ice thickness as a target, nudges free parameters in the basal friction (Eq. 1.12) and basal melt parameterizations (Eq. 1.14), and per construct starts a continuation run with the observed mass change rates from Smith et al. (2020). The second initialization, the 'Flow Enhancement Factor initialization' (abbreviated as 'FEFI'), additionally targets observed ice surface velocities by nudging the flow enhancement factor E (Eq 1.15). The former initialization is used in other CISM applications to the AIS (Van Den Akker et al., 2024; Lipscomb et al., 2021; Berdahl et al., 2023). Other studies, which use the 'Data Assimilation' method to initialize their ice sheet models, include by default the observed ice surface velocities as targets (Bradley and Arthern, 2021; Larour et al., 2012; Cornford et al., 2015; Arthern et al., 2015). Both initializations are tested on their stability. We deem an initialization successful and 'stable' when there is little to no instantaneous model drift once we turn of the inversions and keep our nudged parameters constant, and no significant changes in modelled ice sheet geometry when run forward for 2000 years, similar to what was done by Van Den Akker et al. (2025)

2.4.1 Default initialization (DI)

The default initialization uses Eq 1.12 and Eq 1.14 to initialize an Antarctic Ice sheet in equilibrium, with ice thicknesses approximately matching the observations of Morlighem et al. (2020) and observed thinning/thickening rates (dH/dt) from Smith et al. (2020). At the end of the inversion process, the resulting ice velocities are in good agreement with the observed surface velocities from Rignot et al. (2011). The observed dH/dt is imposed as an additional term in the mass transport equation during the initialization, as described in Van Den Akker et al. (2025). We start the initialization by providing CISM the observed ice thickness from Morlighem et al. (2020) after which the thickness is allowed to evolve. At every following timestep, CISM nudges the free parameter in the friction law (C_c in Eq 1.1) and the ocean temperature correction (δT in Eq 1.13) to decrease the modelled thickness mismatch with the observations. A successful initialization is considered complete when the modelled ice sheet thickness converges; the resulting modelled thickness, surface velocities, grounding line position and basal melt fluxes are close to their observed values; and forward simulations with continued imposed dH/dt display minimal drift. For normal forward simulations, the observed dH/dt is no longer added to the mass transport equation, so that these simulations start with thinning rates equal to the observed thinning rates, as in Van Den Akker et al. (2025).

2.4.2 Flow Enhancement Factor Initialization (FEFI)

Often in ice sheet models, the effective viscosity depends on the strain rates and a flow factor, with the flow factor dependent on the ice temperature via an Arrhenius relation. However, impurities and other factors may also influence the flow factor, hence an enhancement factor E can be introduced to scale the flow factor where necessary.

If E increases, the effective viscosity decreases (Eq. 1.16), which will increase the ice deformation and the ice surface velocities. This inversion changes the vertical structure of the velocity profile, altering the difference between the surface and

https://doi.org/10.5194/egusphere-2025-441
Preprint. Discussion started: 12 March 2025
© Author(s) 2025. CC BY 4.0 License.

basal velocities. Hence, changes in E can make a region more deformation-dominated (as in the Shallow Ice Approximation, or SIA) or sliding-dominated (as in the Shallow Shelf Approximation, or SSA).

We use the three observational datasets listed above as nudging targets; each has different timestamps, resolutions, and uncertainties. We use two (DI) or three (FEFI) free parameters to nudge the modelled present-day ice sheet towards observations. In both cases, the system is underdetermined, i.e. multiple combinations of tuned free parameter values will result in the same or very similar modelled ice sheet. Moreover, the nudging procedure has two degrees of freedom in the FEFI simulations to match observations of observed ice thickness and ice surface velocities. Due to the inconsistent datasets, this might lead to a well-matching thickness thanks to the basal friction inversion, a well-matching ice surface velocity thanks to the FEFI, but physically implausible behavior. The nudging procedure is free, for example, to create sliding or deformation regimes where mathematically preferred, to minimize the difference between observed and modelled surface velocities. The FEFI simulation might therefore have greater skill in representing observations, but for the wrong reasons. Our goal in this study is not directly to simulate the AIS as realistically as possible, but rather to show the impact of common initialization choices on simulations of the future.

2.5 Continuation experiments

We carry out continuation experiments to test the modelled ice sheet evolution sensitivity to the choice of basal friction law, starting from the two initializations described above. We do not apply any further climate forcing (oceanic and atmospheric temperature as well as the surface mass balance are kept constant in time). Each run consists of either 1000 or 2000 model years, depending on the WAIS deglaciated state after 1000 years. We focus on the WAIS due to its greatest dynamic changes in both the observations (Smith et al., 2020) and modelled ice.

The initial state of the modelled AIS will differ slightly if we perform initializations with different friction laws. We would like to start our experiments from the same initial state. Therefore, we rewrite free parameters in the friction laws, C_p and C_c, to allow us to start continuation runs with different basal sliding laws from the same initialized state as was done by Brondex et al. (2017) and Brondex et al. (2019). This has two advantages. First, there are initially no differences in geometry between continuation runs, so all differences can be attributed to the choice of the basal sliding law or the initialization (DI or FEFI). Second, the initialization typically takes about 10,000 model years, while a continuation only requires 1000–2000 yr, saving computational expenses. The details of rewriting the free parameters are described in the supplementary material.

https://doi.org/10.5194/egusphere-2025-441
Preprint. Discussion started: 12 March 2025
© Author(s) 2025. CC BY 4.0 License.

3. Amundsen Sea Embayment

The Amundsen Sea Embayment is presented in Fig.2 . Both PIG and TG are flanked by bedrock above sea level and separated by a small ridge that is well below sea level but has some prominence compared to the troughs on both sides (Fig. 3). The basin boundary (as defined by Zwally et al. (2015) crosses over this ridge. The present-day grounding line is situated at a chokepoint: as it recedes upstream into the troughs, the distance between the left flank of PIG and right flank of TG becomes larger. However, if the grounding line recedes, a shelf can remain in place, locked at the narrow point between the two flanks where the grounding line currently exists.

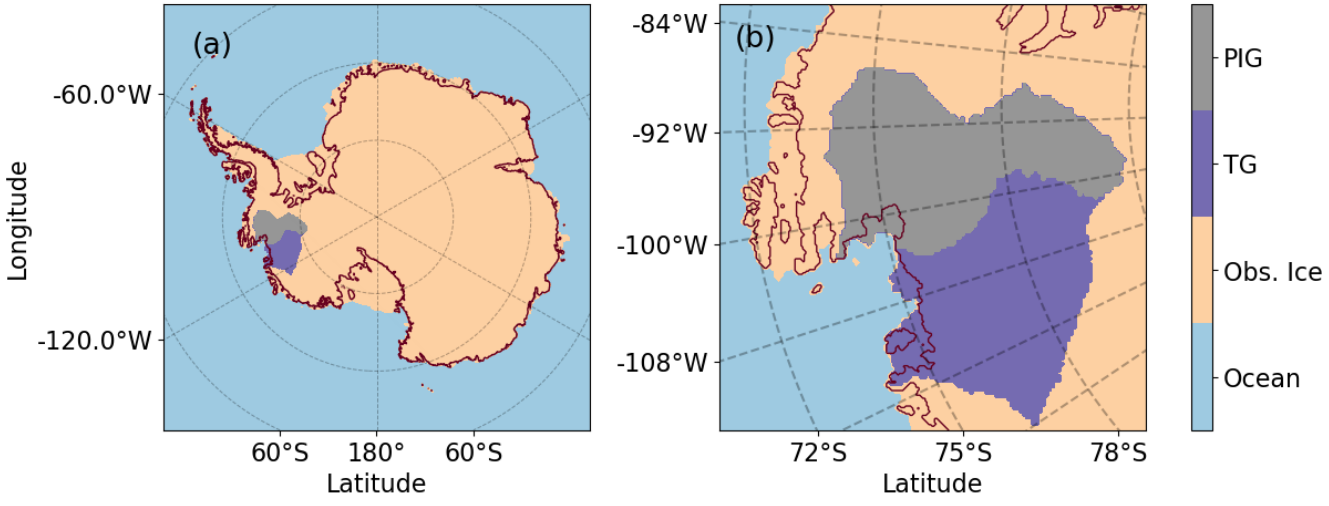

Figure 2. Schematic overview of the modelled area. The Antarctic Ice Sheet (a), with orange denoting the region where ice is observed in the dataset of Morlighem et al. (2020). The observed grounding line (following Morlighem et al. (2020) and applying hydrostatic equilibrium) is shown by a thin red line. The TG basin is shown in purple and the PIG basin in grey, following Zwally et al. (2015). Basin-integrated calculations are applied over these two areas. (b) a close-up of the Amundsen Sea Embayment.

https://doi.org/10.5194/egusphere-2025-441
Preprint. Discussion started: 12 March 2025
© Author(s) 2025. CC BY 4.0 License.

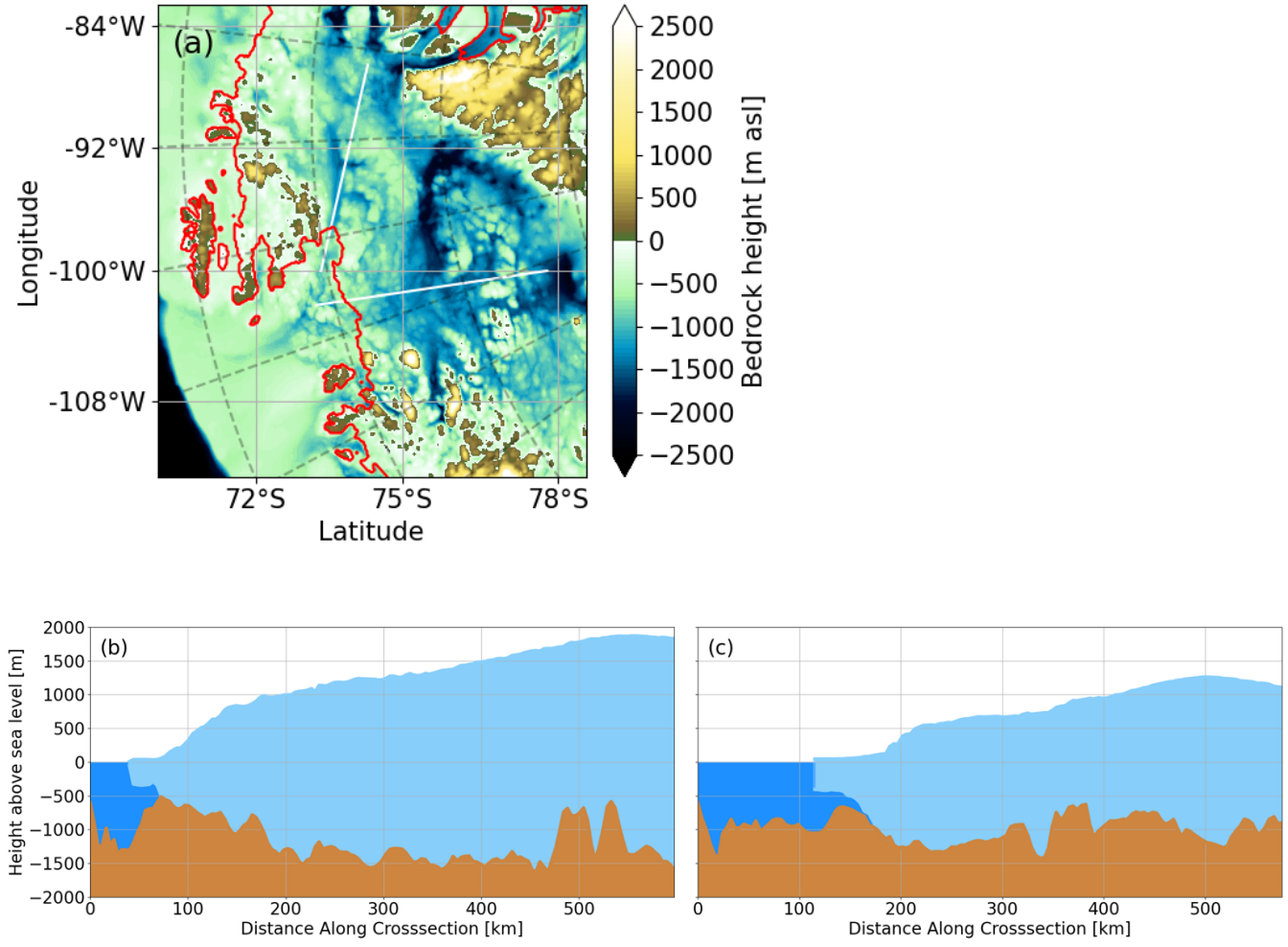

Figure 3. Regional setting. (a) bedrock profile of the Amundsen Sea Embayment with the observed grounding line position, using ice thickness and bedrock height observations from Morlighem et al. (2020) in red. White lines indicate the locations of the cross sections shown below. (Bottom row) cross sections with the ice sheet shown in light blue, the ocean in dark blue, and bedrock in brown. TG in (b) and PIG in (c).

4 Results

In this section, we first show and discuss the modelled present-day ice sheet using the two initialization methods (Sect. 2.4). We highlight key differences and discuss implications of choices made during the initialization. Then we present the unforced future simulations, discussing their different responses to changes in basal friction and showing how these differences are related to the ice sheet geometry and buttressed ice shelves.

https://doi.org/10.5194/egusphere-2025-441
Preprint. Discussion started: 12 March 2025
© Author(s) 2025. CC BY 4.0 License.

4.1 Initial condition evaluation

As a starting point for our forward experiments, we use the two spin-up types described in the previous sections. We evaluate the initial states here.

4.1.1 Default initialization (DI)

Figure 4 shows the initial ice sheet state after the default initialization. The overall thickness bias is low. The regional thickness bias of the East Antarctic Ice Sheet (EAIS) relates to the small observed thickening in central EAIS (Smith et al., 2020), which equals a mass flux similar in magnitude to the local surface mass balance. The RMSE between modelled and observed ice thickness and modelled and observed ice surface velocity are respectively 21.10 m, 135.81 m/yr).

The modelled grounding line position (Fig. 4a) matches the observed position well, with a modest average error of 1.4 km. Surface ice velocities generally agree with observations except for glaciers on the Siple coast, which flow slightly too fast, and the seaward sides of the Filchner-Ronne and Amery ice shelves, where the flow is too slow. Assuming that the observed imposed *dH/dt* is correct, this implies that the ice flux along flowlines in these locations decreases too quickly in CISM. Hence, to retrieve the observed geometry during the inversion, basal melt is decreased. The inverted C_c (Fig. 4c) is generally high in the interior or under slow-moving areas of the ice sheet, and low under outlet glaciers. The inverted ocean temperature perturbations (Fig. 4d) under the larger ice shelves (Filchner-Ronne, Ross and Amery) are generally close to zero with the exception of some positive corrections under the PIG, TG, and Crosson shelves in the ASE region.

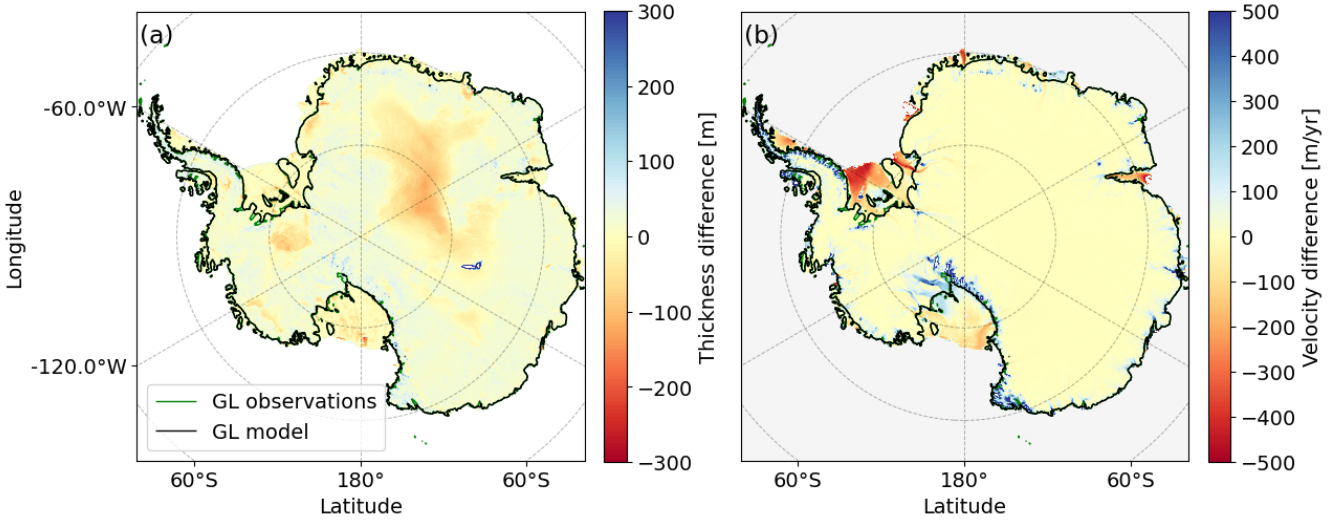

https://doi.org/10.5194/egusphere-2025-441
Preprint. Discussion started: 12 March 2025
© Author(s) 2025. CC BY 4.0 License.

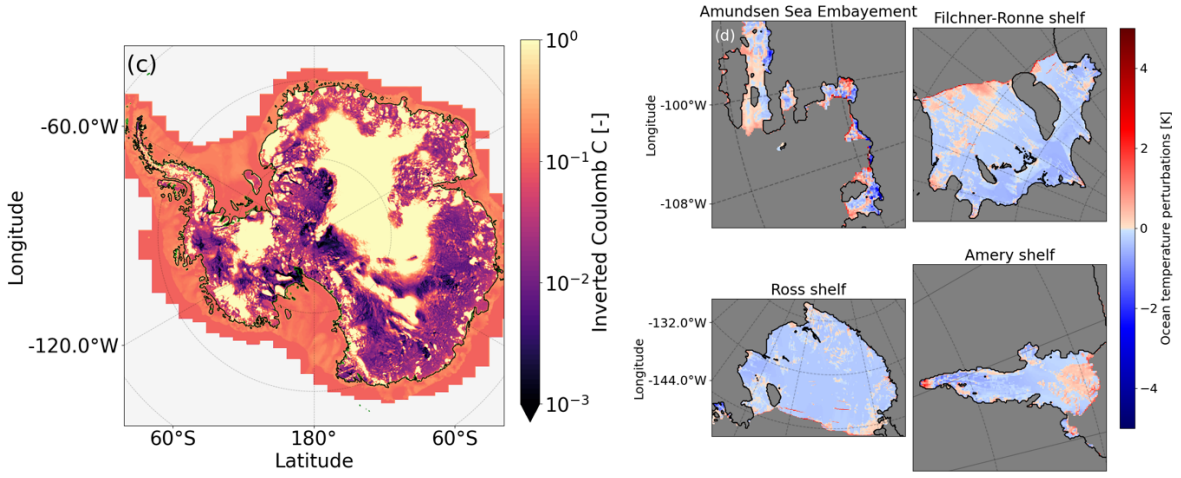

Figure 4. Modelled Antarctic Ice Sheet initialized state with the default inversion. (a) thickness difference with respect to observations (Morlighem et al., 2020). The modelled grounding line is shown in black, and the observed grounding line in green (only visible where it does not overlap with the modelled one). (b) ice surface velocity difference with respect to the observations (Rignot et al., 2011). Positive values indicate regions where CISM overestimates the ice velocities. (c) the inverted C_c from Eq 1.1 using Eq 1.2. and (d) the inverted ocean temperature perturbation under the main shelves.

4.1.2 Flow Enhancement Factor Initialization (FEFI)

Figure 5 shows the ice sheet state after the FEFI 10 kyr initialization. Optimizing for both ice thickness and ice velocity creates a trade-off leading to a slightly increased thickness error and generally a decreased velocity error (RMSE thickness and velocity: 45.99 m, 101 m/yr). The thickness bias in the interior of the EAIS has grown in area and magnitude, showing that either the provided SMB is too low, or the imposed thickening is overestimated. There is no large difference visible in the inverted C_c (Fig. 5c) compared to Fig 4c, and the inverted ocean temperature perturbations show the same pattern as in Fig 4d. Ocean temperature perturbations are generally larger near the calving front and lower in the interior of the shelves, especially for the Filchner-Ronne and Ross shelves. Ice velocities are generally greater in the shelves compared to the default inversion, better matching the observed velocities. This increases the ice flux through the ice shelves, lowers the need for basal melting in the shelf interior, and increases the ice flux at the calving front.

https://doi.org/10.5194/egusphere-2025-441
Preprint. Discussion started: 12 March 2025
© Author(s) 2025. CC BY 4.0 License.

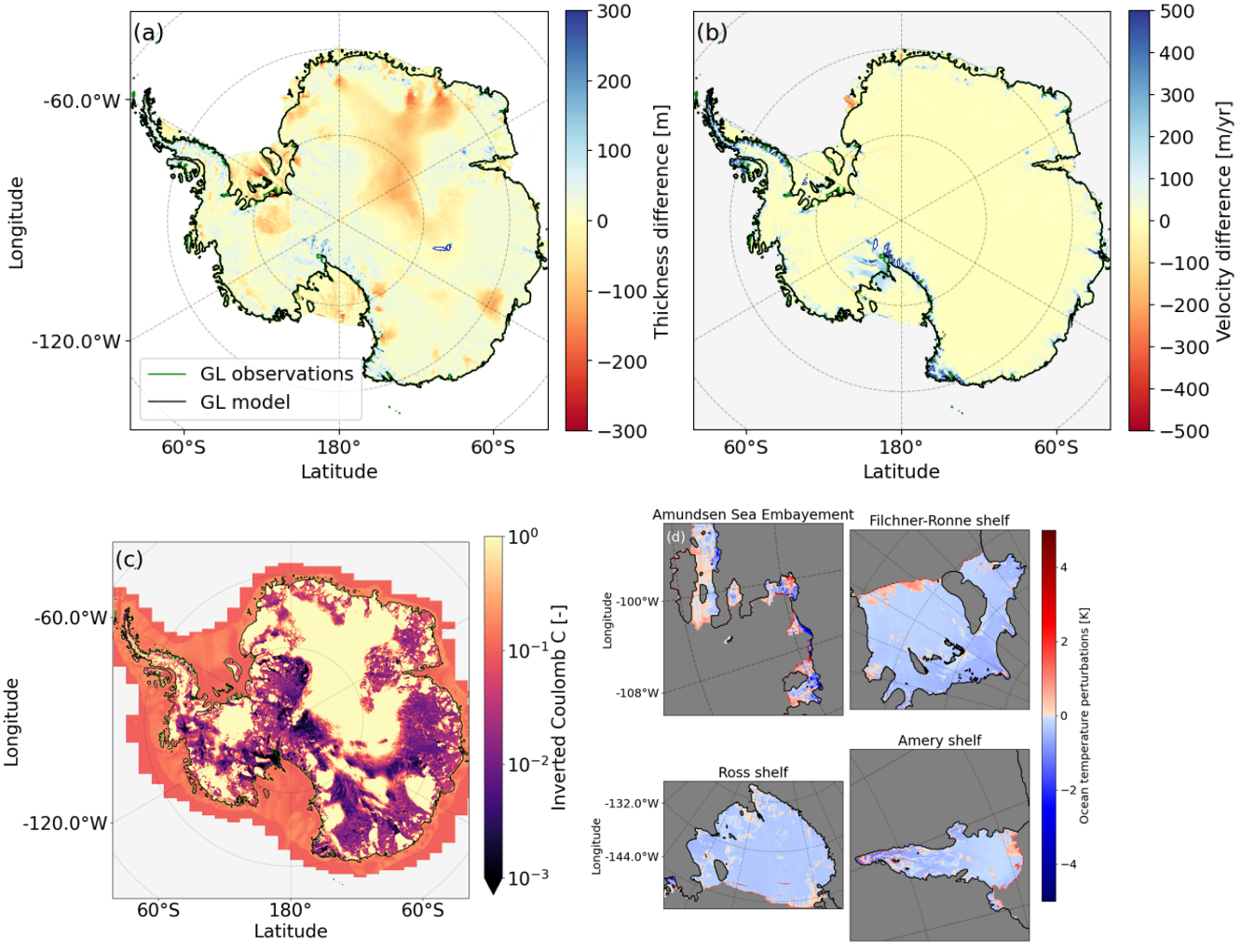

Figure 5. As in Figure 4 but for the flow enhancement factor inversion.

Figure 6 shows the inverted flow enhancement factor and the velocity error change, basal friction change and flow regime change between FEFI and DI simulations for the Amundsen Sea region. First, the flow enhancement factor E in Eq 1.7 is not spatially constant anymore but shows a chaotic pattern in the main flowlines of PIG and TG. PIG and West TG generally weaken (higher E), while East TG stiffens. The velocity differences are due to a local inversion (cell-by-cell E inversion) and a highly non-local influenced variable (ice surface velocities). The basal friction shows a similar speckled pattern. The flow regime is quantified by dividing the ice basal velocity magnitude by the ice surface velocity magnitude. A factor below 1 shows deformation-dominated (SIA) flow, and a factor of 1 shows no vertical velocity shear and therefore sliding-dominated (SSA) flow. Interestingly, in large areas close to the grounding line, the flow regime becomes more deformation-dominated. Where E increases, the ice becomes less viscous, and the flow regime becomes more favorable to deformation.

https://doi.org/10.5194/egusphere-2025-441
Preprint. Discussion started: 12 March 2025
© Author(s) 2025. CC BY 4.0 License.

This is particularly interesting at the Western TG grounding line, where at present the regionally highest ice surface velocities are observed, likely not due to deformation. Sliding is expected to be the dominant regime of a fast-flowing (Antarctic) outlet glacier from standard ice flow theory, and the SSA is widely used as the appropriate stress approximation to model these regions (e.g. Bueler and Brown (2009); Brondex et al. (2019); Gudmundsson et al. (2023); Morlighem et al. (2024). However, Mccormack et al. (2022) modelled the ice flow regime and found a heterogenous pattern of sliding and deformation close to the TG grounding line depended on the flow law used. Observations could provide clarity on the flow regime of the TG grounding line, but it is likely that FEFI tries to compensate the low ice surface velocities by shifting the flow regime towards more deformation, even if sliding dominates in reality. The FEFI initialization and resulting flow enhancement factor and sliding regimes are therefore likely products of our generalized flow law (Eq 1.18), missing modelled physics and/or approximations related to the momentum balances in Eq. 1.11 .

https://doi.org/10.5194/egusphere-2025-441
Preprint. Discussion started: 12 March 2025
© Author(s) 2025. CC BY 4.0 License.

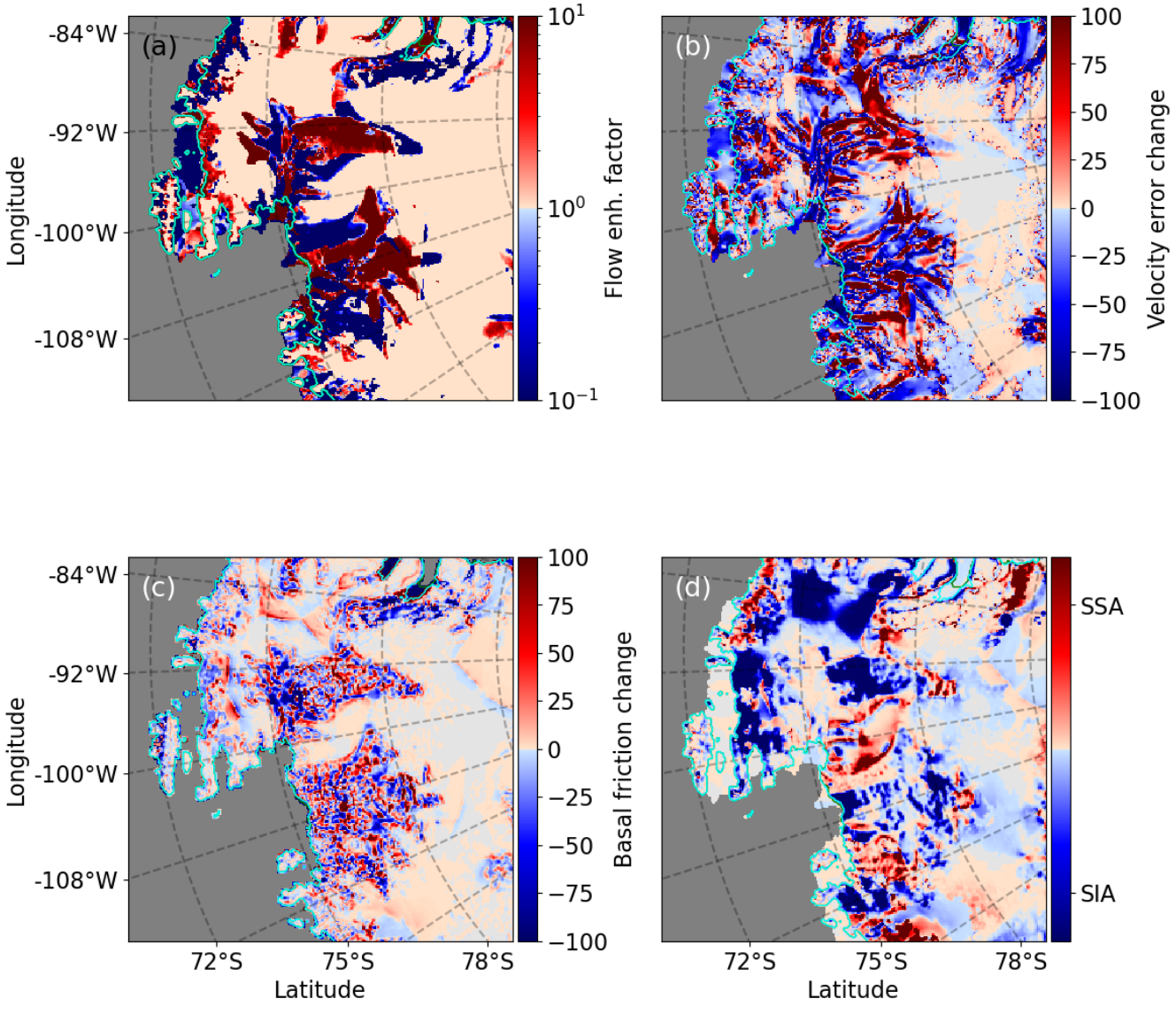

Figure 6. Inverted flow enhancement factor field E in Eq 1.15 (a), the percent differences in velocity error relative to observations from Rignot et al. (2011) (b), the modelled basal friction change between the FEFI and the DI (c), and flow regime change, showing where the ice flow becomes more sliding or deformation dominated in the FEFI simulation (d).

https://doi.org/10.5194/egusphere-2025-441
Preprint. Discussion started: 12 March 2025
© Author(s) 2025. CC BY 4.0 License.

4.2 Modelled unforced evolution of WAIS

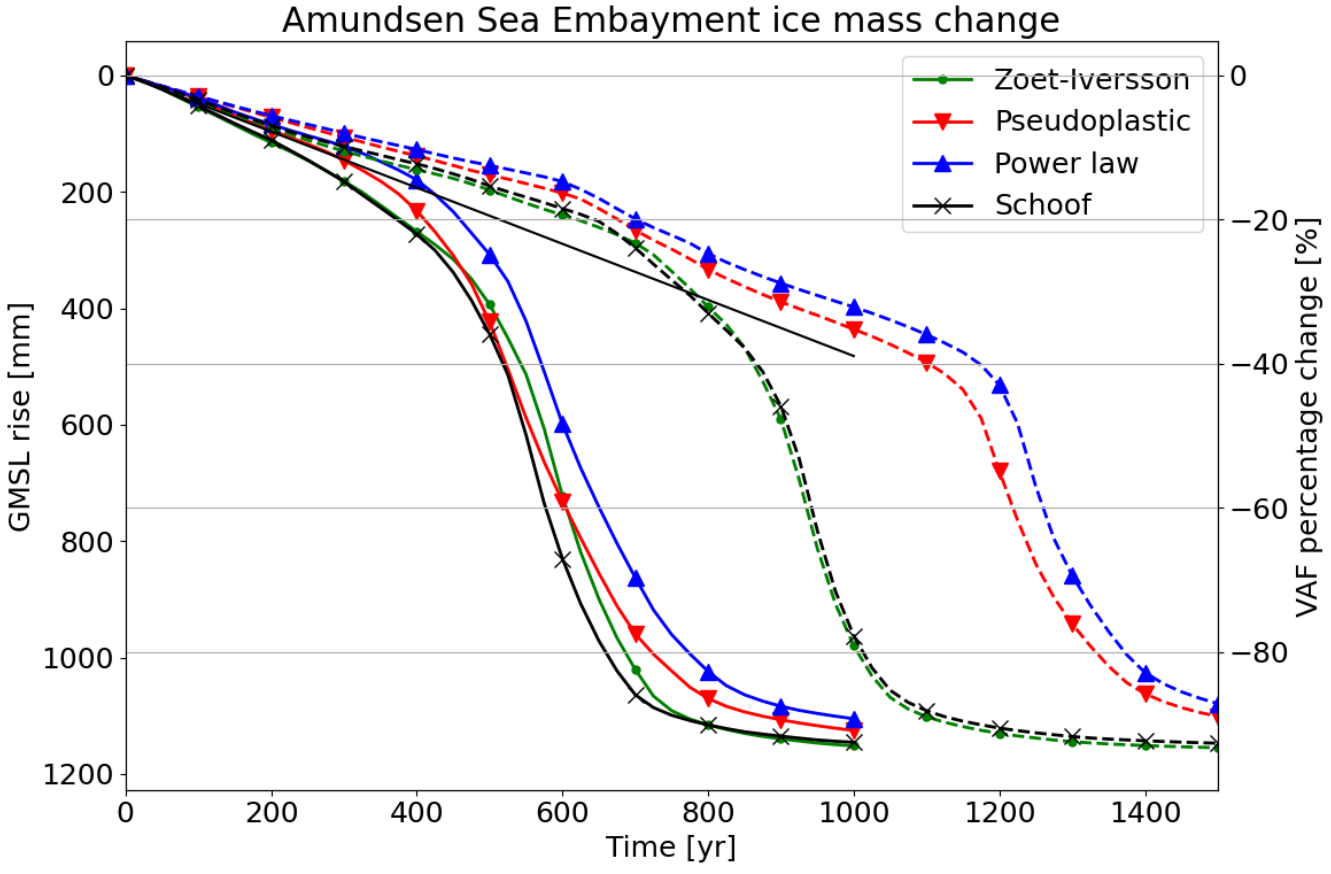

Figure 7. Sea level contributions from the ASE for four different sliding laws with basal friction and ocean temperature perturbation inversion (solid lines) and including the flow enhancement factor inversion (dashed lines). The ice volume above floatation [VAF] percentage change is the loss of ice that can contribute to sea level change (i.e., that is not already floating or present below sea level), relative to the beginning of the simulation, for the basins containing PIG and TG, respectively basin 22 and 21 in Zwally et al. (2015) . The solid black line is the interpolated present-day trend (Smith et al., 2020).

Figure 7 shows the global mean sea level contribution of eight simulations initialized with the mass change rates from Smith et al. (2020). In all simulations, both big glaciers in the ASE eventually collapse and most of the ice volume above floatation (VAF) is released to the ocean. These results are comparable to the results presented in Van Den Akker et al. (2024). In general, the simulations starting from FEFI simulate a longer period of linear mass loss before the start of a steep decline in VAF. For the DI-starting simulations, two stages can be identified. These are i) linear VAF loss similar to the present-day rate and ii) a simultaneous collapse of PIG and TG starting around year 400. For simulations starting from the FEFI, three stages can be

https://doi.org/10.5194/egusphere-2025-441
Preprint. Discussion started: 12 March 2025
© Author(s) 2025. CC BY 4.0 License.

identified, in contrast with the default initialization (solid). These are i) a linear decline in VAF similar to the present-day rate for the first 600 years, ii) PIG collapse for 300 (Schoof and Zoet-Iverson) or 600 (power law and pseudoplastic) years, and iii) TG collapse for approximately 200 years. The maximum rate of sea level rise during the third (TG collapse) phase differs marginally among the eight simulations (4 ± 0.7 mm GMSL per year).

The simulations starting from FEFI exhibit behavior in line with the results of Brondex et al. (2017); Brondex et al. (2019), and Sun et al. (2020): Coulomb sliding (Schoof and Zoet-Iverson) yields earlier and faster collapse than simulations with pseudoplastic and power law sliding). This is in stark contrast to the DI simulations, in which the rate of glacier collapse is much less affected by the choice of the basal friction parameterization. The DI results show the relative non-sensitivity of ice sheet modelling to the specific basal friction law, agreeing with the results of Barnes and Gudmundsson (2022) and Joughin et al. (2024) .

4.2.1 DI: Collapse mechanics and characteristics

We first discuss the results from DI experiments (solid lines in Fig 7), where the collapse rate is relatively insensitive to the choice of basal friction law. Figure 8 shows the elevation profiles of PIG (top row) and TG (bottom row) along the cross-sections shown in Fig. 3. Before the collapse (year 250, first column), the differences in ice sheet geometry and grounding line position for the four sliding laws are small in both glaciers. The end states after the simulated collapse (year 750, last column) are also similar. During the collapse at year 500 (middle column), the shape of the modelled glacier differs. The grounding line is farther, approximately 75 km, receded in the simulation with power law sliding compared to Zoet-Iverson sliding. Typically, the grounding lines of the power law and pseudoplastic law, and the Schoof and Zoet-Iverson law, are grouped together with the exception of the TG collapse. During the TG collapse, the pseudoplastic retreats faster compared to all the other three simulated sliding laws.

The ice shelf and grounded ice just upstream of the modelled grounding line are thicker in the Zoet-Iverson simulation, but inland grounded ice is thicker in the case of power law sliding. This difference in geometry can also be seen in Fig. 9, which shows spatial patterns of thickness change and grounding line position. The grounding line of the power law simulation (top row) is retreated much farther inland compared to the Zoet-Iverson simulation (bottom row) during the collapse at year 500 (middle column). After 750 years, when the collapse has happened and the mass loss slows down, both simulations show a similar geometry again. The small residual shelf at the location of the present-day TG shelf is a remnant of the ocean temperature perturbation tuning. Some cells receive (close to) zero basal melt during the initialization; low melt then persists in the continuation simulations because the ocean conditions are fixed.

https://doi.org/10.5194/egusphere-2025-441
Preprint. Discussion started: 12 March 2025
© Author(s) 2025. CC BY 4.0 License.

These experiments show that the Zoet-Iverson sliding law, with lower friction far upstream of the grounding line, leads to more ice being advected from inland towards the grounding line compared to the power law. As a result, the Zoet-Iverson simulation shows less thinning and retreat near the grounding line, but more inland thinning, compared to the power law simulation. This means that the Zoet-Iverson sliding law results in a smaller but thicker ice shelf in front of the collapsing TG, with a higher buttressing potential and a greater chance to stick to pinning points.

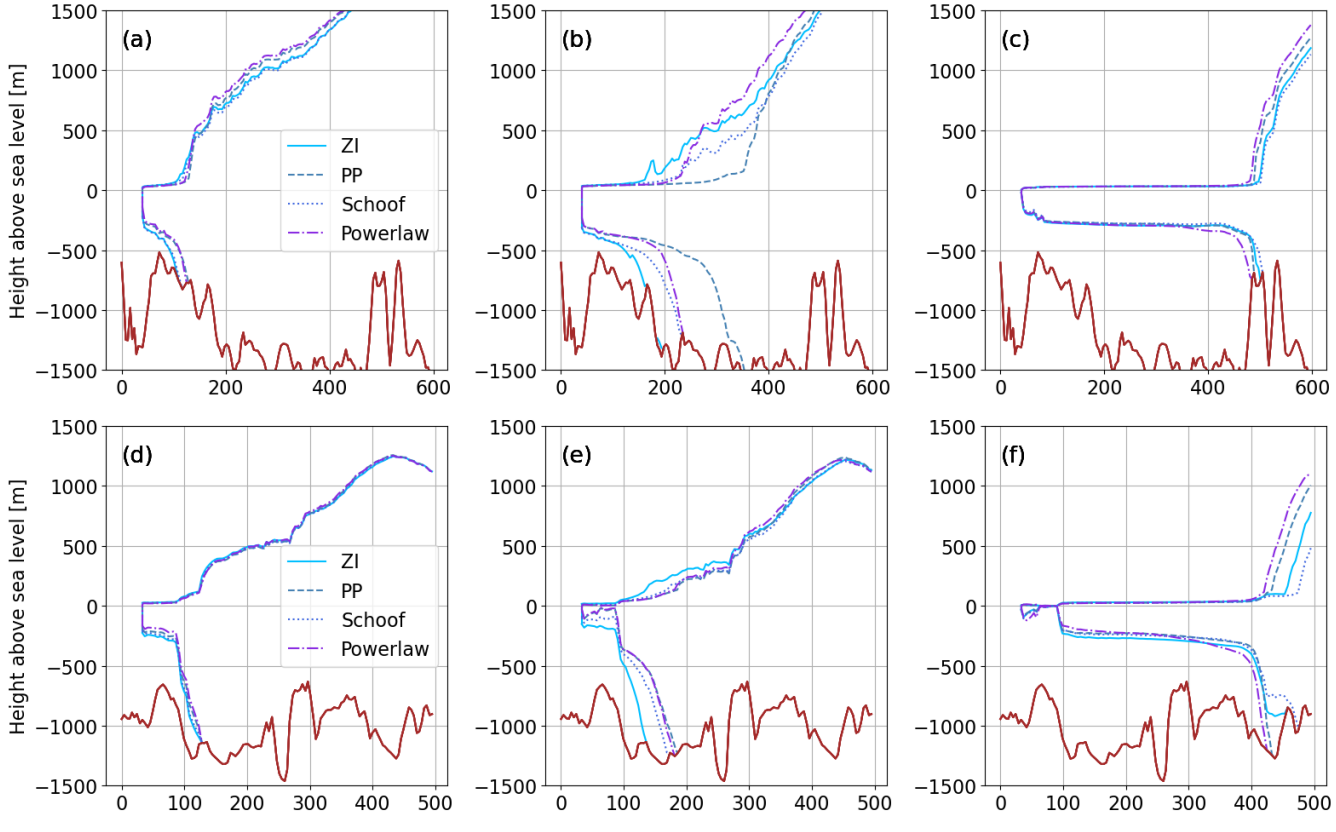

Figure 8. (TOP ROW) Pine Island Glacier along the cross-section shown in Fig 3 at simulation years 250, 500 and 750 for Zoet-Iverson (solid), pseudoplastic (dashed), power law (dashdot) and Schoof (dotted). Bottom row, as a-c for Thwaites.

The similarity between the simulations with Schoof and Zoet-Iverson sliding, and between those with power law and pseudoplastic sliding, can be explained by their similar functional relations between basal velocity and friction, shown in Figure 1. In the rest of this section, we focus on one member from each pair: the Zoet-Iverson law and the power law.

https://doi.org/10.5194/egusphere-2025-441
Preprint. Discussion started: 12 March 2025
© Author(s) 2025. CC BY 4.0 License.

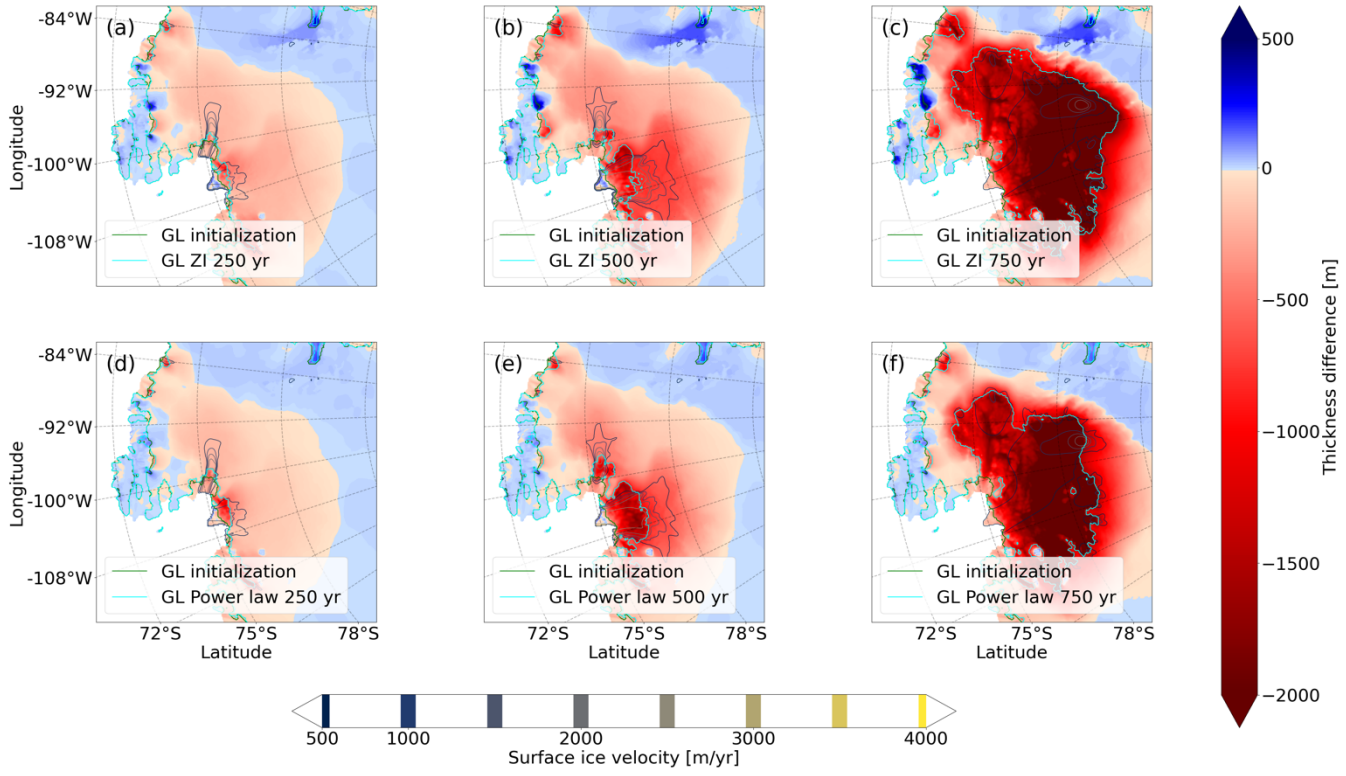

Figure 9. Top row: power law thickness change since the initialization at year 250 (a), 500 (b) and 750 (c), with grounding line position and surface velocity contours. Bottom row: same for Zoet-Iverson.

To explain the difference in collapse mechanism but a similar VAF evolution, we analyze the buttressing of TG and PIG during the collapse. We applied both buttressing quantifications described in section 2.2 to the 250- and 500-year Zoet-Iverson and power law simulation, as shown in Figure 10. Both simulations show a less buttressed Western Thwaites Ice Stream and more buttressed Eastern Thwaites Ice Stream. Moving closer to the calving front decreases the buttressing number. In general, the buttressing close to the grounding line is stronger for the Zoet-Iverson sliding law, according to this method. Little difference can be seen in the confined Pine Island Glacier in both simulations.

The right side of Figure 10 show ice velocity changes in the shelf-kill experiments at years 250 and 500 for the Zoet-Iverson sliding (left column) and power law sliding (right column). A clear pattern is visible. After removal of the ice shelves, grounded ice in the Zoet-Iverson simulation immediately speeds up, significantly more compared to the power law case, at the Thwaites grounding line and farther inland. This indicates that for this specific geometry, a retreating Thwaites Glacier experiences more buttressing with the Zoet-Iverson sliding law than with the power law.

https://doi.org/10.5194/egusphere-2025-441
Preprint. Discussion started: 12 March 2025
© Author(s) 2025. CC BY 4.0 License.

Although the buttressing and acceleration numbers differ (see the supplementary material for a numerical comparison), they both show that the ice shelf that forms in the Zoet-Iverson experiment provides substantially more buttressing than the smaller ice shelf in the power law experiment.

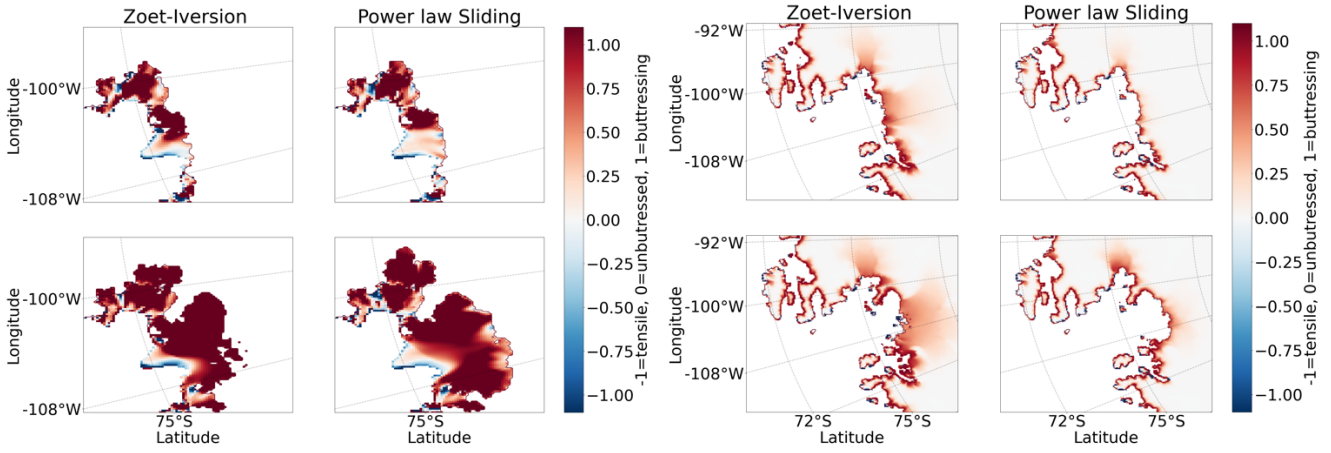

Fig 10. (left four panels) Buttressing number calculated over the floating ice shelves at 250 years (top row) and 500 years (bottom row), for the Zoet-Iverson sliding law (left column) and the power law (right column). (Right four columns) absolute velocity increase after removing the ice shelves at 250 years (top row) and 500 years (bottom row), for the Zoet-Iverson sliding law (left column) and the power law (right column).

There are two mechanisms slowing the flow of grounded ice: buttressing and friction. The combination of these mechanisms determines the grounded ice mass loss. Less friction and more buttressing could result in the same velocities as more friction and less buttressing. This compensation effect is visible in our continuation experiments because the ice shelf in all runs is allowed to persist (no calving front retreat, no forcing applied other than the present-day calibrated ocean temperatures). If the shelf were significantly weaker because of either calving or ocean warming, we would expect the Zoet-Iverson law to yield faster collapse, since the buttressing would not be present to compensate the lower friction.

4.2.2 FEFI: Collapse mechanics and characteristics

In contrast to the default experiments, the simulations starting from the FEFI show a strong sensitivity to the choice of basal friction law. Furthermore, the collapse starts later (initiated around years 800 and 1200 for the Zoet-Iverson and power law cases, respectively), and with a different pattern: Between the period of linear, present-day-like mass loss rate of about ~0.3 mm/yr and the full collapse period with a rate of ~3 mm/yr, there is a period with an intermediate loss rate of about 1-2 mm/yr.

Figure 11 shows a typical snapshot from the collapse phase (the first inflection points in Fig. 1) in both initializations. In the simulations starting from the DI, TG collapses first. In contrast, PIG collapses first in the FEFI simulations, while TG is temporarily stabilized on a bedrock ridge about 40-50 km upstream of the present-day grounding line (white line in Fig 11).

https://doi.org/10.5194/egusphere-2025-441
Preprint. Discussion started: 12 March 2025
© Author(s) 2025. CC BY 4.0 License.

TG reaches this grounding line quickly, before PIG's grounding line starts to recede, but then stabilizes for 800 – 1000 years on a local high in the bedrock (white line in Fig 11.). Once PIG has retreated sufficiently and starts to draw ice from the Thwaites basin, TG starts to collapse. Thus, unlike the DI simulations, PIG initiates ASE deglaciation.

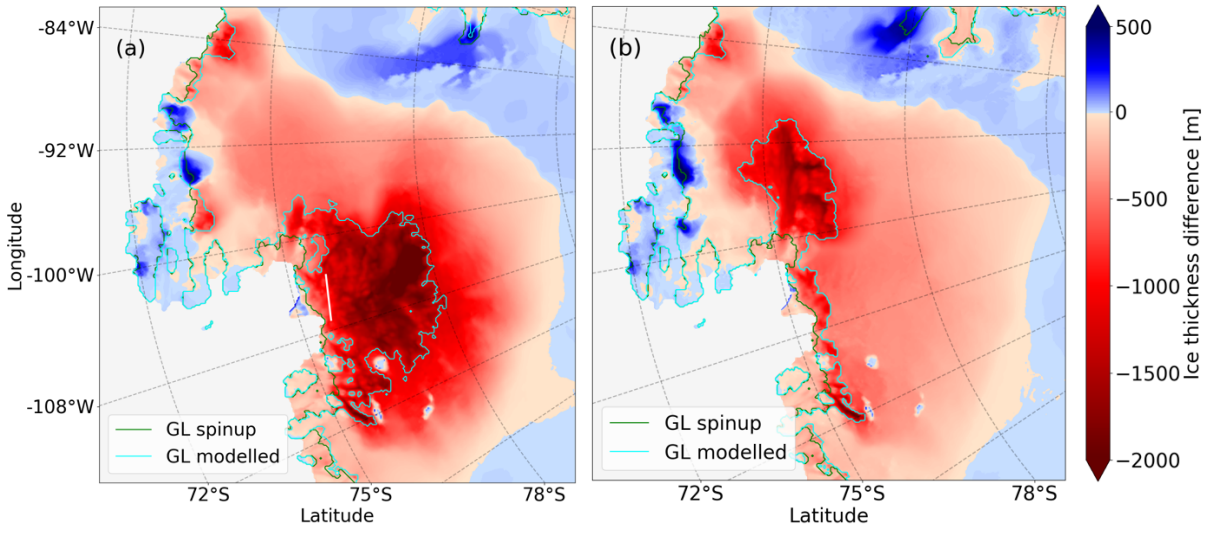

Fig 11. Start of Amundsen Sea ice collapse in simulations with the DI (left) and FEFI (right). Colors indicate the ice thickness difference with respect to the initialization, and the modelled grounding line is shown for the initialization (green) and continuation (cyan). The time snapshots of the left and right panels are respectively for years 575 and 775.

PIG often collapses more slowly than Thwaites Glacier in our simulations. This is shown in Fig. 12. A typical collapse phase of the PIG in these simulations lasts about 300 years when using a Zoet-Iverson sliding law, and up to 800 years when applying power law friction. During this time, the ice sheet loses about 50 centimeters in GMSL equivalent. Since we do not apply surface melting, all losses of grounded ice happen through advection over the grounding lines. A large ice flux over the grounding line initially thickens and strengthens the ice shelf. For Thwaites Glacier, this causes braking effect: a thicker, stronger and more buttressed ice shelf slows down the upstream flow and lowers the ice flux through the grounding line. For PIG, the increased grounding line flux apparently does not lead to a sufficient increase in buttressing to slow down the collapse.

https://doi.org/10.5194/egusphere-2025-441
Preprint. Discussion started: 12 March 2025
© Author(s) 2025. CC BY 4.0 License.

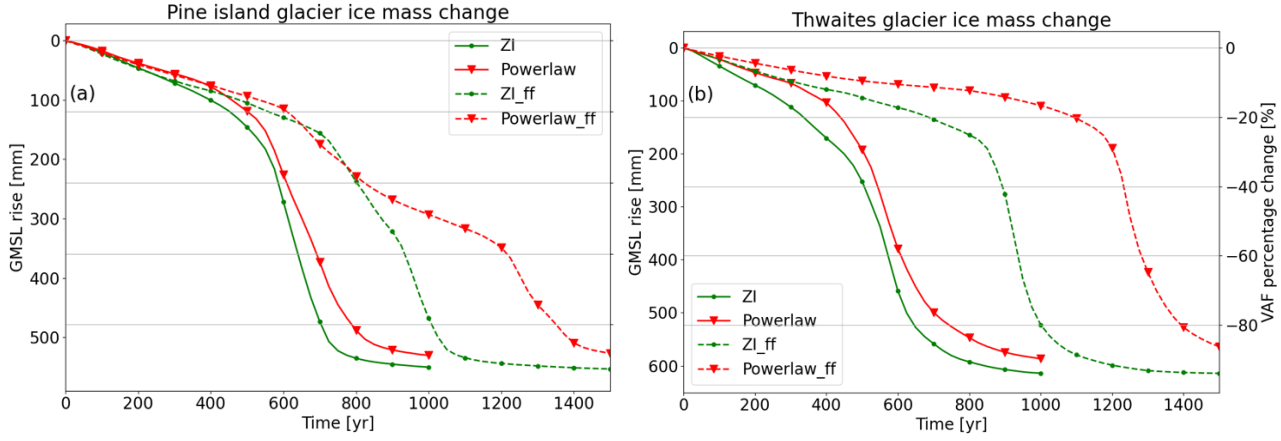

Fig 12. Mass loss shown separately for PIG (left) and TG (right), for both initializations (solid is DI and dashed is FEFI) and for two sliding laws.

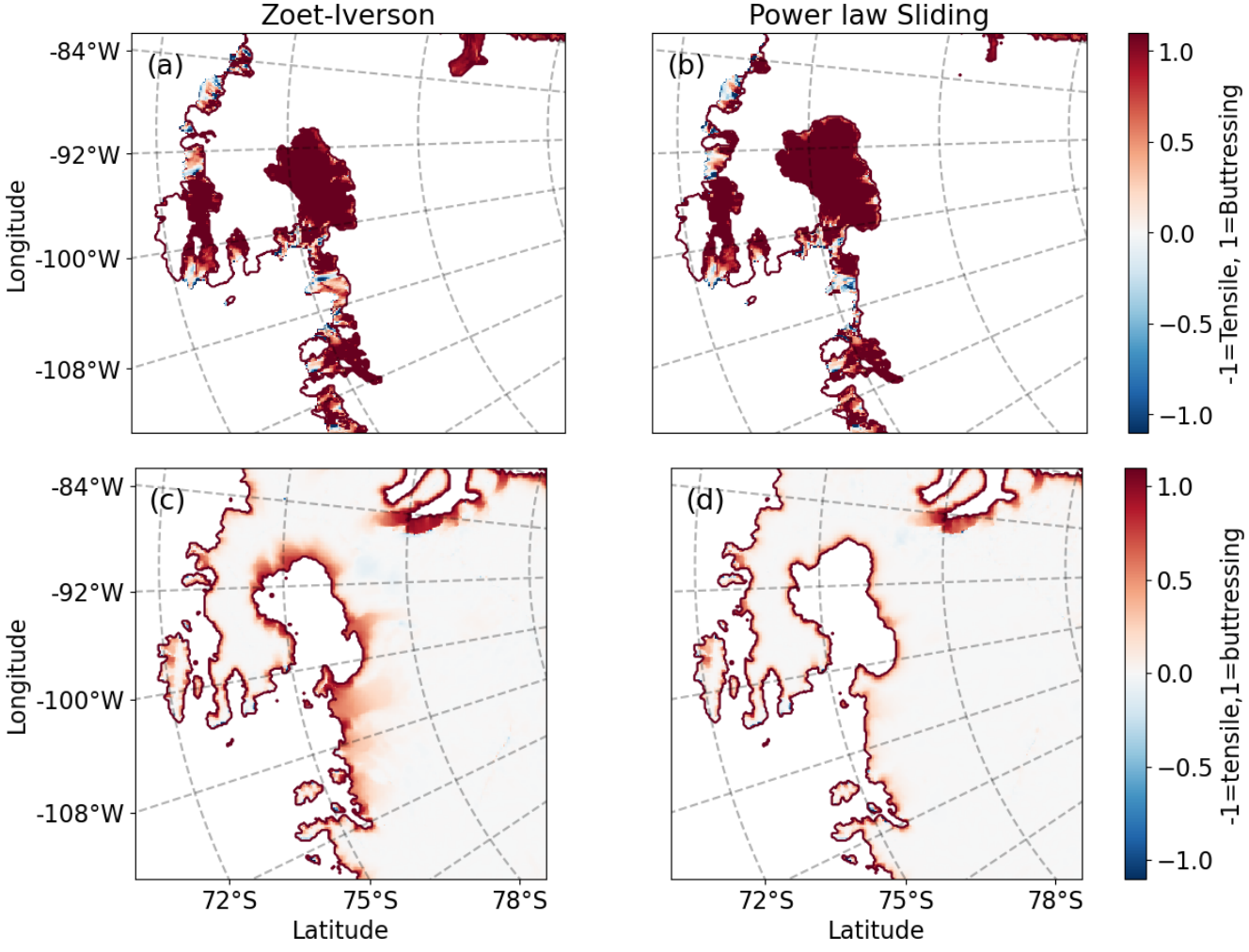

515

https://doi.org/10.5194/egusphere-2025-441
Preprint. Discussion started: 12 March 2025
© Author(s) 2025. CC BY 4.0 License.

Fig 13. Ice shelf removal experiments and buttressing quantification during the FEFI continuations. (Top row) ice accelerations due to the shelf-kill experiments and (bottom row) buttressing quantification for the Zoet-Iverson (left) and the power law (right) simulations.

Figure 13 shows results for the shelf-kill experiments and the buttressing number, repeated with the FEFI initialization. We remove the shelves just before the accelerated collapse begins, at around 775 years into the simulation. We can see that an effect is visible: close to the grounding lines, the simulations with the Zoet-Iverson sliding law have a larger speed-up. In the power law case, removing the shelf hardly matters. However, the difference in acceleration as a reaction to the removal of all floating ice is much smaller for the FEFI initialization, compared to the DI initialization. This is reflected in the similar buttressing numbers for the two sliding laws. Hence, the ice shelves formed during the PIG collapse in the FEFI simulations are weaker than the shelves formed during TG collapses in the DI continuations. At this stage of the FEFI simulations, TG has retreated into a confined embayment with pinning points, with a slightly stronger shelf in the Zoet-Iverson sliding simulation.

4.3 Mass balance comparison

Figure 14 shows the mass balance of the PIG and TG ice shelves for two continuation simulations starting from the different initializations. For TG in both initializations, the integrated basal melt flux is almost equal in magnitude and timing to the integrated grounding line flux. Therefore, the ice shelf hardly grows or shrinks in volume. For PIG, there is a persistent lower integrated grounding line flux compared to the basal melt flux. This means that on average, the ice shelf is losing mass and therefore losing its buttressing potential. When the shelf is unable to buttress the glacier, the collapse is sensitive to the amount of basal friction.

The basal melt is depth-dependent, since the ISMIP6 forcing dataset from Jourdain et al. (2020) has increasing thermal forcing with depth in the ASE. This causes lower ice drafts to melt faster; hence, newly floating cells with deep drafts will receive high basal melt rates. This is a negative feedback on the ice shelf: if the shelf thickens, its base will lie in deeper and warmer water and receive more melt, thinning the shelf.

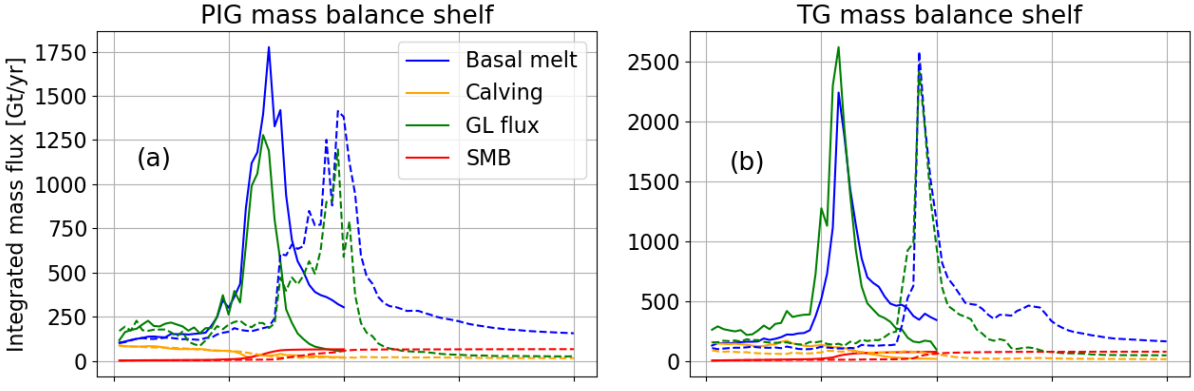

https://doi.org/10.5194/egusphere-2025-441
Preprint. Discussion started: 12 March 2025
© Author(s) 2025. CC BY 4.0 License.

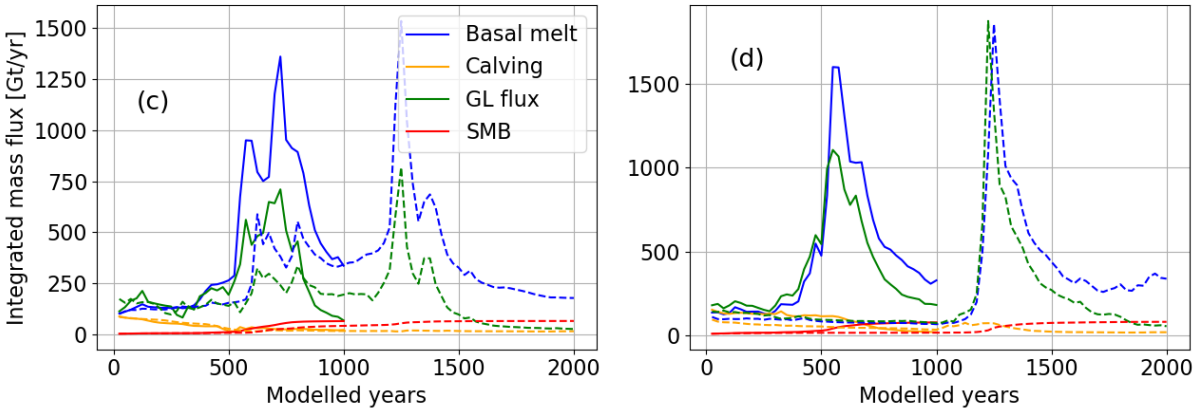

Fig 14. Mass balance of Pine Island (left column) and Thwaites (right column) shelves for the Zoet-Iverson simulation (top row) and the power law (bottom row). Solid lines indicate simulations starting from the default inversion, dashed lines start from the flow enhancement factor inversion.

In summary, the FEFI simulations show more sensitivity to the choice of basal sliding law than the DI simulations. This is related to the existence of a strong buttressing TG shelf at the start of the collapse in the DI simulations, whereas there is no strong buttressing PIG shelf at the start of the collapse in the FEFI simulations. In our simulations, the initialization determines whether the collapse starts with TG or PIG. Therefore, we can initialize the AIS with CISM to be sensitive to the choice of basal friction law or not.

5 Discussion

Our study is consistent with studies arguing that different basal friction parameterizations cause significantly different response (Brondex et al., 2017; Sun et al., 2020; Brondex et al., 2019), and also with studies that claim the opposite (Barnes and Gudmundsson, 2022; Wernecke et al., 2022). We argue that sensitivity to the sliding law depends on the specific geometric setting, e.g. on whether PIG or TG collapses first, and whether the ice shelf can survive and provide buttressing. In our cases, the geometry is sensitive to the initialization. This study was inspired by Berends et al. (2023), who showed that obtaining a similar initial state does not necessarily lead to the same forced retreat in idealized experiments. Furthermore, Berends et al. (2023) showed that choices or even errors in parameterizations and boundary conditions can be compensated by the inversion, which happens in our initializations as well. Both our initializations result in a good representation of the present-day Antarctic Ice Sheet but have a different dynamical response. The flow enhancement factor inversion decreases surface ice velocity errors, but with changes in other tuned parameters and a slightly larger ice thickness error.

The connection between buttressing and basal friction during TG collapse hinges on the survival of the ice shelf that forms during grounding-line retreat. This is in turn determined by the basal melt and calving rates. With respect to calving, we apply

https://doi.org/10.5194/egusphere-2025-441
Preprint. Discussion started: 12 March 2025
© Author(s) 2025. CC BY 4.0 License.

a no-advance calving front at the present-day position. Theoretically, the calving front can move inland, but we use a conservative limit of 1 m ice thickness before ice is allowed to be removed. In practice, this rarely happens. Using a physically-based calving law would likely increase calving rates as the ice thins and the grounding line retreats, and would influence the compensating feedback demonstrated in this study.

With respect to basal melt rates, we apply the ISMIP6 basal melt parameterization (Seroussi et al., 2020) with thermal forcing data from Jourdain et al. (2020). Although this approach provides basal melt fluxes in agreement with observations and other model studies (see Van Den Akker et al. (2024), other approaches — such as including a coupled cavity-resolving (regional) ocean model or a sub-model capturing cavity flow like PICO (Reese et al., 2018c) — could result in basal melt rates that are more physically based and lead to different results. The ISMIP6 parameterization lacks freshwater feedbacks such as the reduced formation of Antarctic Bottom Water (Williams et al., 2016) and cooling of the sea surface (Bintanja et al., 2015). Increases or decreases in future basal melt rate will moderate the effective buttressing of the newly formed shelves. Resolving basal melt rates with a model for ocean circulation in cavities could be an interesting topic for future research.

In this study, we use two initializations to show that the sensitivity of modelled ice mass loss in the ASE to the specific basal friction parameterization varies. One initialization is much more sensitive than the other. This is the first step to concluding that the basal friction parameterization sensitivity is determined by the initialization. However, we show this using a single ice sheet model and two initializations. It would be interesting to repeat this exercise with more ice sheet models and different initialization procedures.

In the FEFI initialization, we tune a basal friction coefficient, the flow enhancement factor, and an ocean temperature perturbation. The latter variable is per definition a perturbation on a dataset, so it does not reflect any observable. The basal friction coefficient and flow enhancement factor relate directly to physical properties of the bedrock and the ice. However, as was stated by Aschwanden et al. (2021), all ice sheet models have incomplete or missing physical processes, and approximate the momentum balance in some way, which leads to parametric uncertainty. The flow enhancement factor tuning is directly influenced by the choice of the momentum balance, and the use of simple generalized flow law (Eq 1.18). Rathmann and Lilien (2022) show that the tuned flow enhancement factor when using Eq 1.18 compensates for more complex ice fabric properties only when the basal friction coefficient is known. This is not the case in our study, so we refrain from interpreting our inverted flow enhancement factor as a physical parameters, but rather as a compensating error. Future work could focus on repeating the experiments done by Rathmann and Lilien (2022), implementing a more complex anisotropic flow law proposed for example by Gillet-Chaulet et al. (2005), and/or simulate the full Stokes momentum balance.

The FEFI initialization results in a modelled AIS with an improved match between modelled ice surface velocities and observations, compared to an initialization only targeting the observed ice thickness. The disadvantage is the addition of

https://doi.org/10.5194/egusphere-2025-441
Preprint. Discussion started: 12 March 2025
© Author(s) 2025. CC BY 4.0 License.

another free, unconstrained, parameter. This makes the system of equations more underdetermined. It would be useful to have observations (like ice velocity depth profiles) on where the ice sheet flow is deformation or sliding dominated, especially in key regions like at the present-day Thwaites grounding line or the pinning point 40 km upstream. Observations could include strain meters in boreholes or surveys of the ice basal velocities in key regions.

6 Conclusion

In this study, we conduct Antarctic Ice Sheet simulations initialized to be consistent with present-day mass loss rates, in which Thwaites Glacier and Pine Island Glacier collapse. We use two initializations; one initialization that solely inverts for basal friction coefficients based on the mismatch between modelled and observed ice thickness, while the other also inverts for a flow enhancement factor based on the mismatch between modelled and observed surface velocities. With the thickness-based initialization, the collapse of Thwaites and Pine Island Glacier is relatively insensitive to the choice of basal friction parameterization, whereas this collapse is strongly sensitive to the basal friction parameterization with the thickness-and-velocity-based inversion. In the former inversion, Thwaites glacier collapses first and exhibits a connection between basal friction and buttressing: increased ice velocities and grounding line fluxes can increase the buttressing. As a result, the sensitivity of our modelled Antarctic Ice Sheet to the choice of basal friction parameterization is determined by the initialization.

This result can explain why some models are sensitive to the choice of basal friction law (Brondex et al., 2017; Sun et al., 2020; Brondex et al., 2019), and others are not (Barnes and Gudmundsson, 2022; Wernecke et al., 2022). We suggest that it is useful for ice sheet modelers to consider this sensitivity when quantifying uncertainty in sea level rise projections, especially uncertainty related to the basal friction parameterization. Reproducing experiments with multiple ice sheet models and different initializations could clarify the importance of the buttressing–basal friction connection. Explorations with more realistic treatments of calving and ocean thermal forcing could also be illuminating. Finally, new (depth) observations on the relative strength of sliding- versus deformation-dominated flow would decrease the degrees of freedom now present in the initialization procedures of ice sheet models.

Code availability

CISM is an open-source code developed on the Earth System Community Model Portal (ESCOMB) Git repository available at https://github.com/ESCOMP/CISM. The specific version used to run these experiments is tagged under https://github.com/ESCOMP/CISM/releases/tag/CISM_basalfriction_buttressing_version .

Data availability

https://doi.org/10.5194/egusphere-2025-441
Preprint. Discussion started: 12 March 2025
© Author(s) 2025. CC BY 4.0 License.

The input dataset, the DI and FEFI simulations, and the output of all experiments shown in Fig 7 can be found on Zenodo at https://doi.org/ 10.5281/zenodo.14719881 (van den Akker, 2025).

Author contributions

TvdA designed and executed the main experiments and the sensitivity analysis. WHL and GRL developed CISM and helped configure the model for the experiments. RSWvdW and WJvdB provided guidance and feedback. TvdA prepared the manuscript, with contributions from all authors.

Financial support

TvdA received funding from the NPP programme of the NWO. WHL and GRL were supported by the NSF National Center for Atmospheric Research, which is a major facility sponsored by the National Science Foundation (NSF) under Cooperative Agreement no. 1852977. Computing and data storage resources for CISM simulations, including the Derecho supercomputer (https://doi.org/10.5065/D6RX99HX), were provided by the Computational and Information Systems Laboratory (CISL) at NSF NCAR. GRL received additional support from NSF grant no. 2045075.

Competing interests

The contact author has declared that none of the authors has any competing interests.

References

Arthern, R. J. and Williams, C. R.: The sensitivity of West Antarctica to the submarine melting feedback, Geophysical Research Letters, 44, 2352-2359, 2017.

Arthern, R. J., Hindmarsh, R. C., and Williams, C. R.: Flow speed within the Antarctic ice sheet and its controls inferred from satellite observations, Journal of Geophysical Research: Earth Surface, 120, 1171-1188, 2015.

Asay-Davis, X. S., Cornford, S. L., Durand, G., Galton-Fenzi, B. K., Gladstone, R. M., Gudmundsson, G. H., Hattermann, T., Holland, D. M., Holland, D., and Holland, P. R.: Experimental design for three interrelated marine ice sheet and ocean model intercomparison projects: MISMIP v. 3 (MISMIP+), ISOMIP v. 2 (ISOMIP+) and MISOMIP v. 1 (MISOMIP1), Geoscientific Model Development, 9, 2471-2497, 2016.

Aschwanden, A., Aðalgeirsdóttir, G., and Khroulev, C.: Hindcasting to measure ice sheet model sensitivity to initial states, The Cryosphere, 7, 1083-1093, 2013.

Aschwanden, A., Fahnestock, M. A., and Truffer, M.: Complex Greenland outlet glacier flow captured, Nature communications, 7, 1-8, 2016.

Aschwanden, A., Bartholomaus, T. C., Brinkerhoff, D. J., and Truffer, M.: Brief communication: A roadmap towards credible projections of ice sheet contribution to sea level, The Cryosphere, 15, 5705-5715, 2021.

Barnes, J. M. and Gudmundsson, G. H.: The predictive power of ice sheet models and the regional sensitivity of ice loss to basal sliding parameterisations: a case study of Pine Island and Thwaites glaciers, West Antarctica, The Cryosphere, 16, 4291-4304, 2022.

Berdahl, M., Leguy, G., Lipscomb, W. H., Urban, N. M., and Hoffman, M. J.: Exploring ice sheet model sensitivity to ocean thermal forcing and basal sliding using the Community Ice Sheet Model (CISM), The Cryosphere, 17, 1513-1543, 2023.

https://doi.org/10.5194/egusphere-2025-441
Preprint. Discussion started: 12 March 2025
© Author(s) 2025. CC BY 4.0 License.

Berends, C. J., Van De Wal, R. S., Van Den Akker, T., and Lipscomb, W. H.: Compensating errors in inversions for subglacial bed roughness: same steady state, different dynamic response, The Cryosphere, 17, 1585-1600, 2023.
Bett, D. T., Bradley, A. T., Williams, C. R., Holland, P. R., Arthern, R. J., and Goldberg, D. N.: Coupled ice/ocean interactions during the future retreat of West Antarctic ice streams, The Cryosphere Discussions, 2023, 1-28, 2023.
Bintanja, R., Van Oldenborgh, G., and Katsman, C.: The effect of increased fresh water from Antarctic ice shelves on future trends in Antarctic sea ice, Annals of Glaciology, 56, 120-126, 2015.
Bradley, A. and Arthern, R.: WAVI. jl: A Fast, Flexible, and Friendly Modular Ice Sheet Model, Written in Julia, AGU Fall Meeting Abstracts, C11A-03,
Brondex, J., Gillet-Chaulet, F., and Gagliardini, O.: Sensitivity of centennial mass loss projections of the Amundsen basin to the friction law, The Cryosphere, 13, 177-195, 2019.
Brondex, J., Gagliardini, O., Gillet-Chaulet, F., and Durand, G.: Sensitivity of grounding line dynamics to the choice of the friction law, Journal of Glaciology, 63, 854-866, 2017.
Budd, W., Keage, P., and Blundy, N.: Empirical studies of ice sliding, Journal of glaciology, 23, 157-170, 1979.
Bueler, E. and Brown, J.: Shallow shelf approximation as a "sliding law" in a thermomechanically coupled ice sheet model, Journal of Geophysical Research: Earth Surface, 114, 2009.
Bulthuis, K., Arnst, M., Sun, S., and Pattyn, F.: Uncertainty quantification of the multi-centennial response of the Antarctic ice sheet to climate change, The Cryosphere, 13, 1349-1380, 2019.
Cornford, S. L., Martin, D., Payne, A., Ng, E., Le Brocq, A., Gladstone, R. M., Edwards, T. L., Shannon, S. R., Agosta, C., and van den Broeke, M. R.: Century-scale simulations of the response of the West Antarctic Ice Sheet to a warming climate, The Cryosphere, 9, 1579-1600, 2015.
Coulon, V., Klose, A. K., Kittel, C., Edwards, T., Turner, F., Winkelmann, R., and Pattyn, F.: Disentangling the drivers of future Antarctic ice loss with a historically calibrated ice-sheet model, The Cryosphere, 18, 653-681, 2024.
Danabasoglu, G., Lamarque, J. F., Bacmeister, J., Bailey, D., DuVivier, A., Edwards, J., Emmons, L., Fasullo, J., Garcia, R., and Gettelman, A.: The community earth system model version 2 (CESM2), Journal of Advances in Modeling Earth Systems, 12, e2019MS001916, 2020.
Das, I., Morlighem, M., Barnes, J., Gudmundsson, G. H., Goldberg, D., and Dias dos Santos, T.: In the Quest of a Parametric Relation Between Ice Sheet Model Inferred Weertman's Sliding-Law Parameter and Airborne Radar-Derived Basal Reflectivity Underneath Thwaites Glacier, Antarctica, Geophysical Research Letters, 50, e2022GL098910, 2023.
Dupont, T. and Alley, R.: Assessment of the importance of ice-shelf buttressing to ice-sheet flow, Geophysical Research Letters, 32, 2005.
Favier, L., Durand, G., Cornford, S. L., Gudmundsson, G. H., Gagliardini, O., Gillet-Chaulet, F., Zwinger, T., Payne, A., and Le Brocq, A. M.: Retreat of Pine Island Glacier controlled by marine ice-sheet instability, Nature Climate Change, 4, 117-121, 2014.
Feldmann, J. and Levermann, A.: Collapse of the West Antarctic Ice Sheet after local destabilization of the Amundsen Basin, Proceedings of the national academy of sciences, 112, 14191-14196, 2015.
Fox-Kemper, B., H.T. Hewitt, C. X., Aðalgeirsdóttir, G., Drijfhout, S. S., Edwards, T. L., Golledge, N. R., Hemer, M., Kopp, R. E., Krinner, G., Mix, A., Notz, D., Nowicki, S., Nurhati, I. S., Ruiz, L., Sallée, J.-B., Slangen, A. B. A., and Yu., Y.: Ocean, Cryosphere and Sea Level Change. In Climate Change 2021: The Physical Science Basis. Contribution of Working Group I to the Sixth Assessment Report of the Intergovernmental Panel on Climate Change Cambridge University Press, Cambridge, United Kingdom and New York, NY, USA, 1211-1362, 2021.
Fürst, J. J., Durand, G., Gillet-Chaulet, F., Tavard, L., Rankl, M., Braun, M., and Gagliardini, O.: The safety band of Antarctic ice shelves, Nature Climate Change, 6, 479-482, 2016.
Gillet-Chaulet, F., Gagliardini, O., Meyssonnier, J., Montagnat, M., and Castelnau, O.: A user-friendly anisotropic flow law for ice-sheet modeling, Journal of glaciology, 51, 3-14, 2005.
Goldberg, D. N.: A variationally derived, depth-integrated approximation to a higher-order glaciological flow model, Journal of Glaciology, 57, 157-170, 2011.
Gudmundsson, G.: Ice-shelf buttressing and the stability of marine ice sheets, The Cryosphere, 7, 647-655, 2013.
Gudmundsson, G. H., Barnes, J. M., Goldberg, D., and Morlighem, M.: Limited impact of Thwaites Ice Shelf on future ice loss from Antarctica, Geophysical Research Letters, 50, e2023GL102880, 2023.

https://doi.org/10.5194/egusphere-2025-441
Preprint. Discussion started: 12 March 2025
© Author(s) 2025. CC BY 4.0 License.

Haseloff, M. and Sergienko, O. V.: The effect of buttressing on grounding line dynamics, Journal of Glaciology, 64, 417-431, 2018.
Joughin, I., Shapero, D., and Dutrieux, P.: Responses of the Pine Island and Thwaites glaciers to melt and sliding parameterizations, The Cryosphere, 18, 2583-2601, 2024.
Joughin, I., Smith, B. E., and Medley, B.: Marine ice sheet collapse potentially under way for the Thwaites Glacier Basin, West Antarctica, Science, 344, 735-738, 2014.
Joughin, I., Smith, B. E., and Schoof, C. G.: Regularized Coulomb friction laws for ice sheet sliding: Application to Pine Island Glacier, Antarctica, Geophysical research letters, 46, 4764-4771, 2019.
Jourdain, N. C., Asay-Davis, X., Hattermann, T., Straneo, F., Seroussi, H., Little, C. M., and Nowicki, S.: A protocol for calculating basal melt rates in the ISMIP6 Antarctic ice sheet projections, The Cryosphere, 14, 3111-3134, 2020.
Larour, E., Seroussi, H., Morlighem, M., and Rignot, E.: Continental scale, high order, high spatial resolution, ice sheet modeling using the Ice Sheet System Model (ISSM), Journal of Geophysical Research: Earth Surface, 117, 2012.
Leguy, G., Asay-Davis, X., and Lipscomb, W.: Parameterization of basal friction near grounding lines in a one-dimensional ice sheet model, The Cryosphere, 8, 1239-1259, 2014.
Leguy, G. R., Lipscomb, W. H., and Asay-Davis, X. S.: Marine ice sheet experiments with the Community Ice Sheet Model, The Cryosphere, 15, 3229-3253, 2021.
Lipscomb, W. H., Leguy, G. R., Jourdain, N. C., Asay-Davis, X., Seroussi, H., and Nowicki, S.: ISMIP6-based projections of ocean-forced Antarctic Ice Sheet evolution using the Community Ice Sheet Model, The Cryosphere, 15, 633-661, 2021.
Lipscomb, W. H., Price, S. F., Hoffman, M. J., Leguy, G. R., Bennett, A. R., Bradley, S. L., Evans, K. J., Fyke, J. G., Kennedy, J. H., and Perego, M.: Description and evaluation of the community ice sheet model (CISM) v2. 1, Geoscientific Model Development, 12, 387-424, 2019.
McCormack, F., Warner, R., Seroussi, H., Dow, C., Roberts, J., and Treverrow, A.: Modeling the deformation regime of Thwaites Glacier, West Antarctica, using a simple flow relation for ice anisotropy (ESTAR), Journal of Geophysical Research: Earth Surface, 127, e2021JF006332, 2022.
Morlighem, M., Goldberg, D., Barnes, J. M., Bassis, J. N., Benn, D. I., Crawford, A. J., Gudmundsson, G. H., and Seroussi, H.: The West Antarctic Ice Sheet may not be vulnerable to marine ice cliff instability during the 21st century, Science Advances, 10, eado7794, 2024.
Morlighem, M., Rignot, E., Binder, T., Blankenship, D., Drews, R., Eagles, G., Eisen, O., Ferraccioli, F., Forsberg, R., and Fretwell, P.: Deep glacial troughs and stabilizing ridges unveiled beneath the margins of the Antarctic ice sheet, Nature Geoscience, 13, 132-137, 2020.
Nowicki, S. M., Payne, A., Larour, E., Seroussi, H., Goelzer, H., Lipscomb, W., Gregory, J., Abe-Ouchi, A., and Shepherd, A.: Ice sheet model intercomparison project (ISMIP6) contribution to CMIP6, Geoscientific model development, 9, 4521-4545, 2016.
Pattyn, F. and Morlighem, M.: The uncertain future of the Antarctic Ice Sheet, Science, 367, 1331-1335, 2020.
Payne, A. J., Nowicki, S., Abe-Ouchi, A., Agosta, C., Alexander, P., Albrecht, T., Asay-Davis, X., Aschwanden, A., Barthel, A., and Bracegirdle, T. J.: Future sea level change under coupled model intercomparison project phase 5 and phase 6 scenarios from the Greenland and Antarctic ice sheets, Geophysical Research Letters, 48, e2020GL091741, 2021.
Pollard, D. and DeConto, R.: Description of a hybrid ice sheet-shelf model, and application to Antarctica, Geoscientific Model Development, 5, 1273-1295, 2012.
Rathmann, N. M. and Lilien, D. A.: Inferred basal friction and mass flux affected by crystal-orientation fabrics, Journal of Glaciology, 68, 236-252, 2022.
Reese, R., Winkelmann, R., and Gudmundsson, G. H.: Grounding-line flux formula applied as a flux condition in numerical simulations fails for buttressed Antarctic ice streams, The Cryosphere, 12, 3229-3242, 2018a.
Reese, R., Gudmundsson, G. H., Levermann, A., and Winkelmann, R.: The far reach of ice-shelf thinning in Antarctica, Nature Climate Change, 8, 53-57, 2018b.
Reese, R., Albrecht, T., Mengel, M., Asay-Davis, X., and Winkelmann, R.: Antarctic sub-shelf melt rates via PICO, The Cryosphere, 12, 1969-1985, 2018c.
Reese, R., Garbe, J., Hill, E. A., Urruty, B., Naughten, K. A., Gagliardini, O., Durand, G., Gillet-Chaulet, F., Gudmundsson, G. H., and Chandler, D.: The stability of present-day Antarctic grounding lines–Part 2: Onset of irreversible retreat of

https://doi.org/10.5194/egusphere-2025-441
Preprint. Discussion started: 12 March 2025
© Author(s) 2025. CC BY 4.0 License.

Amundsen Sea glaciers under current climate on centennial timescales cannot be excluded, The Cryosphere, 17, 3761-3783, 2023.
Rignot, E., Mouginot, J., and Scheuchl, B.: Ice flow of the Antarctic ice sheet, Science, 333, 1427-1430, 2011.
Robinson, A., Goldberg, D., and Lipscomb, W. H.: A comparison of the stability and performance of depth-integrated ice-dynamics solvers, The Cryosphere, 16, 689-709, 2022.
Schoof, C.: The effect of cavitation on glacier sliding, Proceedings of the Royal Society A: Mathematical, Physical and Engineering Sciences, 461, 609-627, 2005.
Schoof, C.: Ice sheet grounding line dynamics: Steady states, stability, and hysteresis, Journal of Geophysical Research: Earth Surface, 112, 2007a.
Schoof, C.: Marine ice-sheet dynamics. Part 1. The case of rapid sliding, Journal of Fluid Mechanics, 573, 27-55, 2007b.
Seroussi, H., Nakayama, Y., Larour, E., Menemenlis, D., Morlighem, M., Rignot, E., and Khazendar, A.: Continued retreat of Thwaites Glacier, West Antarctica, controlled by bed topography and ocean circulation, Geophysical Research Letters, 44, 6191-6199, 2017.
Seroussi, H., Nowicki, S., Payne, A. J., Goelzer, H., Lipscomb, W. H., Abe-Ouchi, A., Agosta, C., Albrecht, T., Asay-Davis, X., and Barthel, A.: ISMIP6 Antarctica: a multi-model ensemble of the Antarctic ice sheet evolution over the 21st century, The Cryosphere, 14, 3033-3070, 2020.
Seroussi, H., Pelle, T., Lipscomb, W. H., Abe-Ouchi, A., Albrecht, T., Alvarez-Solas, J., Asay-Davis, X., Barre, J. B., Berends, C. J., and Bernales, J.: Evolution of the Antarctic Ice Sheet over the next three centuries from an ISMIP6 model ensemble, Earth's Future, 12, e2024EF004561, 2024.
Smith, B., Fricker, H. A., Gardner, A. S., Medley, B., Nilsson, J., Paolo, F. S., Holschuh, N., Adusumilli, S., Brunt, K., and Csatho, B.: Pervasive ice sheet mass loss reflects competing ocean and atmosphere processes, Science, 368, 1239-1242, 2020.
Sun, S., Pattyn, F., Simon, E. G., Albrecht, T., Cornford, S., Calov, R., Dumas, C., Gillet-Chaulet, F., Goelzer, H., and Golledge, N. R.: Antarctic ice sheet response to sudden and sustained ice-shelf collapse (ABUMIP), Journal of Glaciology, 66, 891-904, 2020.
Tsai, V. C., Stewart, A. L., and Thompson, A. F.: Marine ice-sheet profiles and stability under Coulomb basal conditions, Journal of Glaciology, 61, 205-215, 2015.
van den Akker, T., Lipscomb, W. H., Leguy, G. R., Bernales, J., Berends, C., van de Berg, W. J., and van de Wal, R. S.: Present-day mass loss rates are a precursor for West Antarctic Ice Sheet collapse, EGUsphere, 2024, 1-25, 2024.
van den Akker, T., Lipscomb, W. H., Leguy, G. R., Bernales, J., Berends, C. J., van de Berg, W. J., and van de Wal, R. S.: Present-day mass loss rates are a precursor for West Antarctic Ice Sheet collapse, The Cryosphere, 19, 283-301, 2025.
Weertman, J.: On the sliding of glaciers, Journal of glaciology, 3, 33-38, 1957.
Wernecke, A., Edwards, T. L., Holden, P. B., Edwards, N. R., and Cornford, S. L.: Quantifying the impact of bedrock topography uncertainty in Pine Island Glacier projections for this century, Geophysical Research Letters, 49, e2021GL096589, 2022.
Williams, G., Herraiz-Borreguero, L., Roquet, F., Tamura, T., Ohshima, K., Fukamachi, Y., Fraser, A., Gao, L., Chen, H., and McMahon, C.: The suppression of Antarctic bottom water formation by melting ice shelves in Prydz Bay, Nature communications, 7, 12577, 2016.
Winkelmann, R., Martin, M. A., Haseloff, M., Albrecht, T., Bueler, E., Khroulev, C., and Levermann, A.: The Potsdam parallel ice sheet model (PISM-PIK)–Part 1: Model description, The Cryosphere, 5, 715-726, 2011.
Zoet, L. K. and Iverson, N. R.: A slip law for glaciers on deformable beds, Science, 368, 76-78, 2020.
Zwally, H. J., Li, J., Robbins, J. W., Saba, J. L., Yi, D., and Brenner, A. C.: Mass gains of the Antarctic ice sheet exceed losses, Journal of Glaciology, 61, 1019-1036, 2015.